Title
Fault Tolerant Autonomous Lateral Control for Heavy Vehicles

Authors
Talbot, Craig Matthew
Papadimitriou, Iakovos
Tomizuka, Masayoshi

Publication Date
2004-08-01

CALIFORNIA PATH PROGRAM
INSTITUTE OF TRANSPORTATION STUDIES
UNIVERSITY OF CALIFORNIA, BERKELEY

Fault Tolerant Autonomous Lateral Control for Heavy Vehicles

Craig Matthew Talbot
Iakovos Papadimitriou
Masayoshi Tomizuka
University of California, Berkeley

California PATH Research Report
UCB-ITS-PRR-2004-24

This work was performed as part of the California PATH Program of the University of California, in cooperation with the State of California Business, Transportation, and Housing Agency, Department of Transportation; and the United States Department of Transportation, Federal Highway Administration.

Final Report for Task Order 4233

August 2004

ISSN 1055-1425

PROJECT TITLE:

FAULT TOLERANT AUTONOMOUS LATERAL CONTROL FOR HEAVY VEHICLES

Craig Matthew Talbot
Iakovos Papadimitriou
Masayoshi Tomizuka

Mechanical Engineering Department
UNIVERSITY OF CALIFORNIA at BERKELEY

Final Report for TO 4233

November 2003

EXECUTIVE SUMMARY

This report summarizes the research results of TO4233, “Fault Tolerant Autonomous Lateral Control for Heavy Vehicles”. This project represents a continuing effort of PATH’s research on Automated Highway Systems (AHS) and more specifically in the area of heavy vehicles. Research on the lateral control of heavy vehicles for AHS has been going on at PATH since 1993. MOU129, “Steering and Braking Control of Heavy Duty Vehicles” was the first project and it was followed by MOU242, “Lateral Control of Commercial Heavy Duty Vehicle”. Both projects were concerned mostly with the theoretical portion of the problem, i.e. model development, analysis of the dynamic model from the lateral control point of view, and the lateral controller designs. The first experimental results were shown in MOU289 (MOU313), “Lateral Control of Heavy Duty Vehicles for Automated Highway Systems”, where the theoretical model was validated and calibrated to the dynamic behavior of an actual tractor-semitrailer vehicle, which was obtained and instrumented. In addition, preliminary closed-loop experiments were performed. A more comprehensive study on a large variety of control strategies was presented in MOU385 and TO4201, “Robust Lateral Control of Heavy Duty Vehicles”. More specifically, three types of nonlinear and adaptive controllers for lateral control of heavy vehicles were analyzed theoretically and compared experimentally.

All the research efforts mentioned above have been extremely valuable for the development of automated highway vehicles; however they assume the existence of a fully operational magnet-magnetometer scheme. To be more specific, all the results are based on the assumption that each heavy vehicle is equipped with two banks of magnetic sensors, one mounted on the front bumper and the other mounted on the rear bumper of the trailer. The road is also implanted with equally spaced magnets whose magnetic field is used to measure the vehicle’s lateral deviation from the road centerline (“lane-keeping control”). Up to now, no heavy-vehicle-related report has discussed the case of vehicle lateral performance under the existence of faults. This problem is very important, since safety and reliability are the primary requirements for the success of AHS. This report addresses the problem of fault tolerant control of heavy vehicles by proposing a secondary system that implements “autonomous vehicle following” instead of “lane-keeping”.

The principle of the autonomous following lies on the fact that the controlled vehicle monitors its lateral location relative to the preceding vehicle, and adjusts the steering input accordingly, in order to follow the preceding vehicle's trajectory. By the same token, in a platoon of vehicles, autonomous following implies that all the vehicles of the platoon follow the lead (i.e. the very first) vehicle's trajectory. Clearly, autonomous following assumes that the lead vehicle, either in manual or in automatic mode, achieves satisfactory lane-keeping. The thrust of the method is that no road infrastructure is required; hence the lane keeping performance does not rely on the magnet-magnetometer system. Instead, it relies mainly on a sensor (either vision-based or radar-based) that monitors the rear end of the preceding vehicle. In this report, after presenting and analyzing the vehicle dynamics, the autonomous following scheme will be shown in detail and the hardware and software (controller) requirements will be discussed. We propose the use of a laser scanning radar and a probabilistic filtering algorithm in order to extract accurate information from the raw sensor data.

It has to be noted at this point that the concept of lateral autonomous following has been analyzed in the past and researchers have concluded that one of its major drawbacks is that in a platoon of vehicles the lateral error propagates along the platoon if the control strategy relies merely on the laser scanning radar. However, in this report we propose a solution to this problem by the addition of inter-vehicle communication. More specifically, we mathematically explain the lateral error propagation, we introduce the concept of lateral platoon stability and we show that, by use of inter-vehicle communication, lateral platoon stability, that is, prevention of lateral error propagation, can be achieved. It should be mentioned, that communication delay is accounted for and it is shown that the limitations that it poses can be overcome by careful selection of the control law timing.

Finally, we present some preliminary experimental results. Because of the unavailability of the heavy vehicles, all of the tests were conducted on passenger vehicles. Also, due to the early termination of the project there was no opportunity to test the actual communication system; however it was made possible to emulate the behavior of the laser scanning radar and that of the communication system to a certain extent. More specifically, we used the magnet/magnetometer scheme and emulated the performance of the laser scanning radar by hardcoding the look-ahead distance and the sampling rate to the values that the laser scanning radar would operate at. We also introduced a time delay, in the magnetometer measurements in order to emulate the communication delay.

Although, we recognize that further testing is required, we believe that these preliminary results are quite encouraging and show that the autonomous following scheme is very promising as a means of substituting the magnet/magnetometer scheme when the latter is malfunctioning.

ABSTRACT

This report is concerned with the problem of fault-tolerant lateral control of heavy vehicles operating on highways. First, the lateral dynamics of two-unit vehicles are presented with the assumptions of negligible pitch, yaw and vertical motion. The complex nonlinear model, which is derived, is then simplified to a linear time invariant system. For single-unit vehicles, the derivation of the equations of motion follows intuitively from the two-unit vehicle dynamics.

Next, the problem of lateral autonomous following within a platoon of vehicles is considered. It is shown that the use of sensors that monitor the preceding vehicle's relative lateral position is enough to achieve lateral control for a pair of vehicles, provided that certain limitations are taken into account. For a platoon of multiple vehicles, the lateral error propagation is a serious issue that can be solved if performance is compromised. The use of inter-vehicle communication is proposed in order to recover platoon stability and satisfactory performance. The communication delay is taken into account and it is shown that, under certain circumstances, the communicated data essentially eliminates the interconnection among the vehicles. Simulations for both passenger and tractor-semi-trailer vehicles illustrate the analytical results.

Finally, the experimental setup for automated platooning is presented and several implementation issues are examined. Experimental results are also discussed.

TABLE OF CONTENTS

LIST OF FIGURES

1. INTRODUCTION

Automated Highway Systems (AHS) have lately gained significant attention. For several years now, after the successful implementation and commercialization of conventional and adaptive cruise control techniques, the research community has put a lot of effort in fully automating the driving process, not only in passenger cars, but also in heavy vehicles, so that the traffic throughput is increased as much as possible, [4].

The most common way to face this complicated control problem is to decouple it into two sub-problems; (i) one involving longitudinal control and (ii) the other dealing with lateral control. The cruise control techniques offer the basic solution to the longitudinal control problem, and research currently focuses on refining the control techniques and dealing with reliability issues. Specifically, a large portion of research activities in this area has to do with fault detection and identification as well as degraded mode control, [30]. On the other hand, there is no commercial product for lateral guidance, and the lateral control problem is still a subject of ongoing research. It can be divided into two major categories; (i) lane keeping and (ii) lane changing. Lane changing is still at its infancy, although the concepts of trajectory planning, [11, 19, 24] and obstacle avoidance, [1, 14, 15, 28, 31] – often borrowed from robotics – have contributed to significant progress. The focus is mainly on theoretical aspects of the problem and very few experiments have been successfully conducted, [5, 20,21, 23, 33]. On the other hand, lane-keeping techniques are already quite advanced mainly due to the use of the road infrastructure.

1.1 Infrastructure-Dependent Techniques

One infrastructure-dependent approach to lateral guidance involves the use of video cameras that monitor the vehicle's position relative to the lane markers. This approach, suggested by the European and Japanese research community mainly, has proved to be quite efficient in laboratory environment, [9]. The video camera images, after being processed to output the vehicle's position, are fed into a computer, which controls a steering actuator. The entire configuration essentially implements the well-known "measure-process-act" scheme in order to achieve lane-keeping control.

For the conversion from the camera images to the vehicle's position, several approaches have been proposed. For example, a model-driven approach hypothesizes a possible curvature, subtracts it from the parallelized low-resolution image, and tests to see how well the hypothesized curvature has "straightened" the image. The vehicle's lateral offset relative to the lane center is then calculated according to the calculated road curvature. An important attribute of this technique is that as long as visible features run parallel to the road, this technique exploits them to determine road curvature, [29]. Alternatively, based on certain assumptions, [2], a computer vision system can analyze specific regions to identify and extract the features of interest. It assumes a fixed or smoothly varying lane width and thereby limits its search to almost-parallel lane markers. Then, road geometry reconstruction is based on shape assumptions, such as no discontinuities in curvature changes.

As far as controller design is concerned, Choi *et al.* designed a PI - controller using yaw rate feedback, in order to account for the steering actuator delay and the side-slip. Yaw rate information was generated by an algorithm that processed the data that was detected by a vision system. The controller showed reasonable combination of performance and passenger comfort although the authors admitted that the image processing algorithm delay introduced performance limitations, [8]. Kosecka *et al.* analyzed the role of this delay, related it to the look-ahead distance of the video cameras and came up with an output feedback lead-lag controller that was experimentally tested, [22]. They also discussed the use of a real-time observer and showed that, not only does it reduce the noise inherent in the sensor measurements, but it also provides an accurate vehicle state estimation, thus circumventing the image processing delay.

Vision-based lane keeping is infrastructure-dependent in the sense that it requires great consistency in terms of lane-marker painting. This means that in cases where lane markers are not drawn or there are several lane markers due to construction, there is increased probability that the vision-based system will fail. Another limitation is the fact that video cameras are sensitive to weather conditions. Several algorithms have been developed to deal with decreased visibility in rain or fog [3], however the solution to this problem is still in its infancy. The considerations mentioned above render vision-based lane-keeping a moderate solution to the lateral control problem, at least as a primary lateral control system.

California PATH's approach to lateral control is highly infrastructure dependent as well. It requires magnets implanted in the center of each lane and magnetic field

sensors (which will hereafter be called magnetometers) installed on the vehicle. The measured magnetic field intensity is then proportional to the distance between the sensors and the magnets. Assuming that the vertical distance between them remains constant, it can be inferred that the measured magnetic field intensity is proportional to the lateral distance between the sensors and the road centerline. This distance will hereafter be called lateral error. Hence, the magnetometer measurements, after being converted to lateral error measurements by a processing algorithm, are fed into a computer, which controls a steering actuator, see Fig. 1.1. It is noted that the accelerometer and the yaw rate gyrometer are used for lane changing and for sensor fusion purposes. Further details on the magnet-magnetometer scheme as well as its design features can be found in [35].

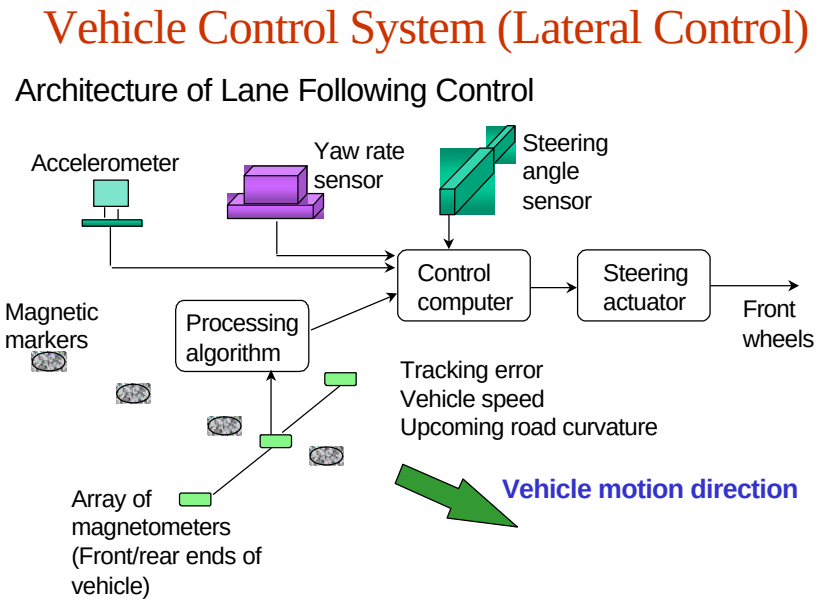

Fig. 1.1: Lane-keeping control architecture.

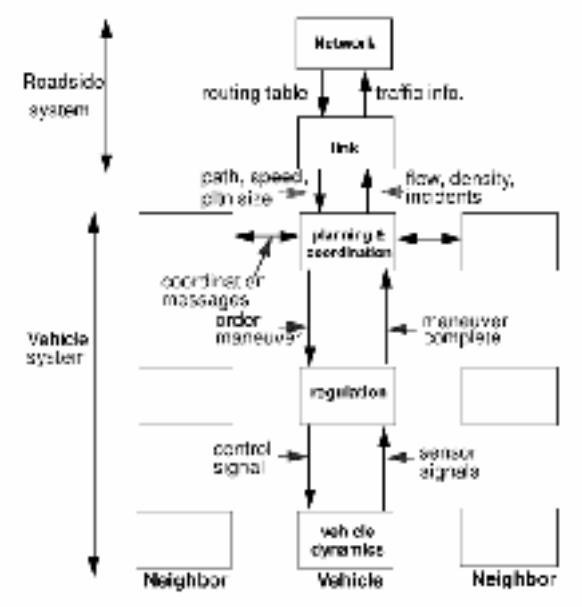

Fig. 1.2: PATH AHS Architecture.

California PATH's research efforts resulted in the National Automated Highway Systems Consortium (NAHSC) Demo 1997 on the I-15 lanes in San Diego, USA, which set the landmark for Intelligent Vehicle Highway Systems. During the demo, a platoon of 8 fully automated vehicles traveled at a distance of *6m* from each other and at highway speeds, thus demonstrating that both longitudinal and lateral control is feasible.

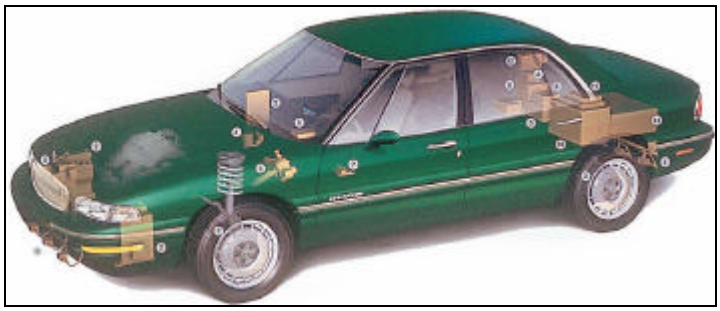

1. Magentometers
2. Computer controlled braking
3. Radar
4. Computer controlled throttle
5. Computer controlled steering
6. Head-up display
7. Acceleration/yaw & pitch rate sensors
8. Vehicle-to-vehicle data transmission
9. Human/machine interface computer
10. Lateral computer
11. Longitudinal computer
12. Sensor/actuators

Fig. 1.3: The test vehicle used by PATH.

Since then, California PATH focused on deployment issues concerning the safety and reliability of the magnetometer based system. The problem was addressed from two different ways; (i) through design of fault detection and identification techniques [30, 34], and (ii) through design of robust and fault tolerant controllers [35]. The former approach implements the scheme detect-identify-reconfigure. More specifically, the installation of multiple sensors to measure the same quantity or the estimation of a quantity through a

model essentially builds system redundancy. Hence, by first monitoring the comparison of the measured variables (residuals), one can detect if there is a sensor fault in the system (detection). With the proper choice of the redundancy techniques and the calculated residuals, it is possible to identify which sensor is faulty (fault identification). The last stage is the reconfiguration of the controller parameters so that it accounts for the faulty sensor. The implicit assumption in this case is that only one sensor is faulty. On the other hand, fault tolerant control techniques are not concerned with the failures themselves; instead, the controller is designed to be insensitive to the changes that a sensor fault introduces. In other words, the closed loop system is designed to be *robust* to the uncertainty introduced by the possible failures.

In the heavy vehicle area, research on lateral control was initiated in 1993 with projects emphasizing on the theoretical aspects, such as model development, analysis of the dynamic model from the lateral control point of view, and the lateral controller designs, [6]. Implementation was achieved in 1998 with a tractor-semitrailer vehicle, [17]. Several magnetometer based control techniques were implemented and achieved satisfactory performance even at highway speeds, [18, 37].

1.2 Problem Formulation

From all of the above, it is clear that the lateral control problem has been solved to a large extent, but there is still plenty of room for improvement when it comes to dealing with system faults. The fact that an inconsistency can result in fatalities poses a big question as to the feasibility of such a project. Moreover, the development cost of such infrastructure-based techniques as well as the maintenance cost is quite large. This motivates for a robust automated lateral control system that is completely independent of infrastructure.

An idea that has gained a lot of attention is termed “autonomous following” and it pertains to the act of monitoring a vehicle’s position not relative to the road centerline, but relative to the preceding vehicle. This technique essentially creates an “electronic tow-bar” and does not require road infrastructure. White and Tomizuka proposed an autonomous following system for trucks by use of a laser scanning radar that monitors the relative lateral position, [38]. Lu and Tomizuka implemented a similar scheme on passenger vehicles, [27]. In Europe, a vision-based system and a trajectory-based approach were suggested in the scope of the CHAUFFEUR Project at DaimlerChrysler,

[13]. Also, within the PRAXITELE Project, INRIA implemented a similar method to develop an electronic tow-bar for passenger cars, [10]. However, the problem that arises in all these techniques is that *lateral platoon stability* is not guaranteed.

Platoon stability is the term used to imply uniform boundedness of the system errors. In the longitudinal (or lateral) direction, this means that any spacing (or lateral) error at some point in the platoon does not propagate along the rest of the platoon. Swaroop and Hedrick defined string stability for interconnected nonlinear systems and proposed a parameter adaptation law to ensure longitudinal platoon stability, [36]. The control strategy that they suggested assumed that the distance from the preceding vehicle would be measured and that the longitudinal velocity and acceleration of the lead vehicle would be communicated to the rest of the platoon. The same system configuration was used by Lee et al., who proposed a two-layer control concept and successfully implemented it in a 4-vehicle platoon, [25]. Gehring and Fritz experimentally tested a similar design on trucks, [12]. Chien and Ioannou avoided the use of inter-vehicle communication by introducing a speed-dependent spacing policy, but achieved platoon stability for large spacing among vehicles only, [7].

Therefore, in the longitudinal direction, platoon stability has been addressed extensively. This is not the case when it comes to lateral platoon stability. To the best of the authors' knowledge, although researchers recognize the fact that by merely monitoring the rear end of the preceding vehicle will result in the propagation of the lateral error along the platoon, they have not mathematically developed a solution that will ensure lateral platoon stability. Hence, the problem that this research addresses can be formulated as follows:

Problem:

Analyze, design and implement an autonomous following system for two-unit vehicles that will ensure lateral platoon stability.

The solution of the problem mentioned above will provide a backup system in case of failure of the conventional magnet-magnetometer based scheme or even a primary cost-efficient system provided that its performance is satisfactory.

1.3 Outline of Report

The remainder of this report is organized as follows. Chapter 2 deals with the dynamic model of two-unit vehicles (tractor-semitrailers) and single-unit vehicles (passenger cars) in a unified way. The analysis of single-unit vehicles was required, because, as explained later, it has not been made possible to experimentally test the control scheme on two-unit vehicles. Chapter 3 is involved with the control design. Lateral platoon stability is defined in order to study the lateral error propagation along a platoon of vehicles and inter-vehicle communication is suggested in order to combine platoon stability with performance. Chapter 4 presents the hardware and software setup and the experimental results related to autonomous following. Finally, Chapter 5 provides a summary and suggestions for future work.

2. ANALYSIS OF VEHICLE DYNAMICS

In this chapter the vehicle's dynamic equations of motion are derived. The analysis is conducted for a two-unit vehicle and then it is shown how these equations collapse into the set of equations that describe the motion of a single-unit vehicle.

The chapter is organized as follows: first, the assumptions that will allow for a simple, yet accurate model of the vehicle are presented, and the kinematic equations that will be useful for the model derivation are explained. The road-tire interaction and the equations that describe it are introduced. Next, the equations of motion are derived using Lagrange's method. Finally, a detailed analysis of the system is presented and several model simplifications are attempted.

2.1 Assumptions

As mentioned above, we deal with a two-unit (tractor-trailer) vehicle as shown in the figure below.

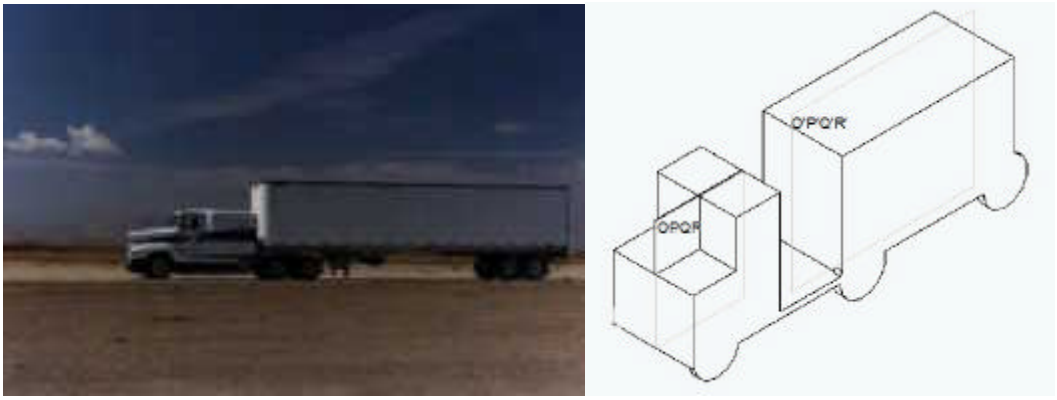

Fig. 2.1: Two-unit vehicle (actual and schematic)

The following assumptions are made:

1. Planes *OPQR* and *O'P'Q'R'* are planes of geometric symmetry. The center of gravity (c.g.) of the tractor and the trailer are located on plane *OPQR* and *O'P'Q'R'* respectively.
2. The road is bumpless, has zero slope and the vehicle is not subject to large longitudinal accelerations. Hence, pitch motion and vertical motion are neglected.

3. The vehicle does not negotiate turns of high curvature profile. Thus, roll motion is also neglected.
4. Each wheel plane is perpendicular to the road plane, that is, the wheel camber angle is *0* and thus the lateral force due camber thrust is *0*.
5. The wheels on each axle are parallel to each other. In addition, only the wheels of the tractor's front axle are steerable.

These assumptions greatly simplify the system since they allow the use of planar dynamics and the omission of the suspension system. Yet they capture quite accurately the lateral behavior of the vehicle in nominal highway operation. The vehicle parameters that will be of use are shown in the table below. The reader is encouraged to consult Fig. 2.2 as well in order to better understand the meaning of each vehicle parameter.

Table 2.1: Parameters of the vehicle model

Parameter	Description
m_1	Tractor mass
m_2	Trailer mass
d_1	Distance between tractor's C.G. and fifth wheel (hitch)
d_3	Distance between trailer's C.G. and fifth wheel (hitch)
l_1	Distance between tractor's C.G. and front wheel axle
l_2	Distance between tractor's C.G. and rear wheel axle
l_3	Distance between fifth wheel (hitch) and trailer's rear axle
T_{w1}	Tractor front axle width
T_{w2}	Tractor rear axel width
T_{w3}	Trailer rear axle width
I_{z1}	Tractor yaw moment of inertia (vertical direction)
I_{z2}	Trailer yaw moment of inertia (vertical direction)
m	Road adhesion coefficient
C_{af}	Cornering stiffness of tractor front wheel
C_{ar}	Cornering stiffness of tractor rear wheel (4 tires)
C_{at}	Cornering stiffness of trailer rear wheel (4 tires)
C_{lf}	Longitudinal stiffness of tractor front wheel
C_{lr}	Longitudinal stiffness of tractor rear wheel (4 tires)
C_{lt}	Longitudinal stiffness of trailer rear wheel (4 tires)
r_{wi}	Wheel radius (i = 1,2,…,6)
I_{wi}	Wheel moment of inertia (i = 1,2,…,6)

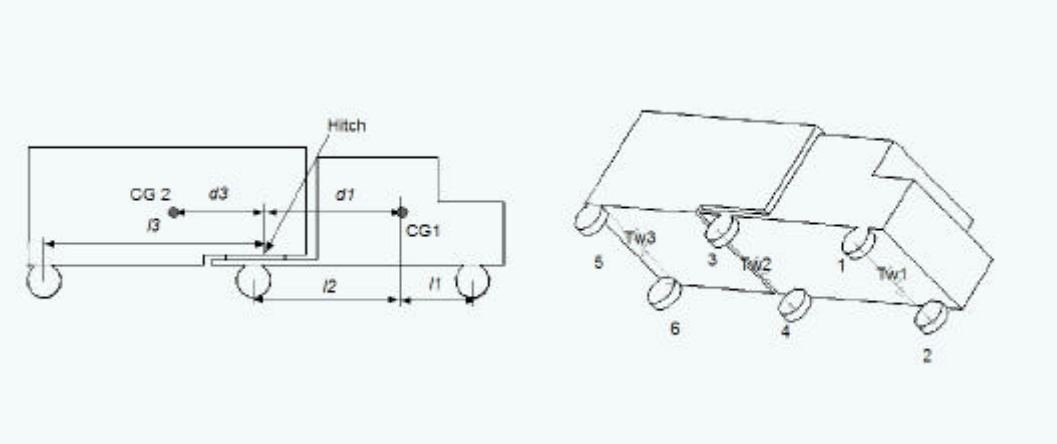

Fig. 2.2: Two-unit vehicle parameters

2.2. Kinematic Equations

In this section, the coordinate frames that will facilitate the derivation of the model are presented. Specifically, the following right-handed coordinate frames are defined:

- The inertial or globally fixed coordinate frame X_nY_n.
- The tractor coordinate frame X_uY_u. This frame is fixed to the tractor's c.g., which means that it translates and rotates with the tractor. The X_u-axis positive direction corresponds to the longitudinal traveling direction of the tractor.
- The trailer coordinate frame X_tY_t. This frame is fixed to the trailer's c.g. Again the X_t-axis positive direction corresponds to the longitudinal traveling direction of the trailer.
- The road reference coordinate frame X_rY_r. The origin of this frame is defined as the intersection of the road centerline and the line that connects the center of the road-curve with the c.g. of the tractor. The X_r-axis is the tangent line of the road-curve at the origin with positive direction pointing towards the tractor's traveling direction. The Y_r-axis positive direction is chosen so that it forms a right-handed coordinate frame.
- The tire coordinate frames X_{wi},Y_{wi}, $i=1,2,..6$. These frames are fixed to the wheels' geometric centers. The positive X_{wi}-direction points towards each wheel's traveling direction.

The coordinate frames are shown in the figure below and the variables of interest are shown in the table that follows. Note that this is an unrealistic position of the vehicle, but it is very helpful since all the angles that are defined are positive in this figure.

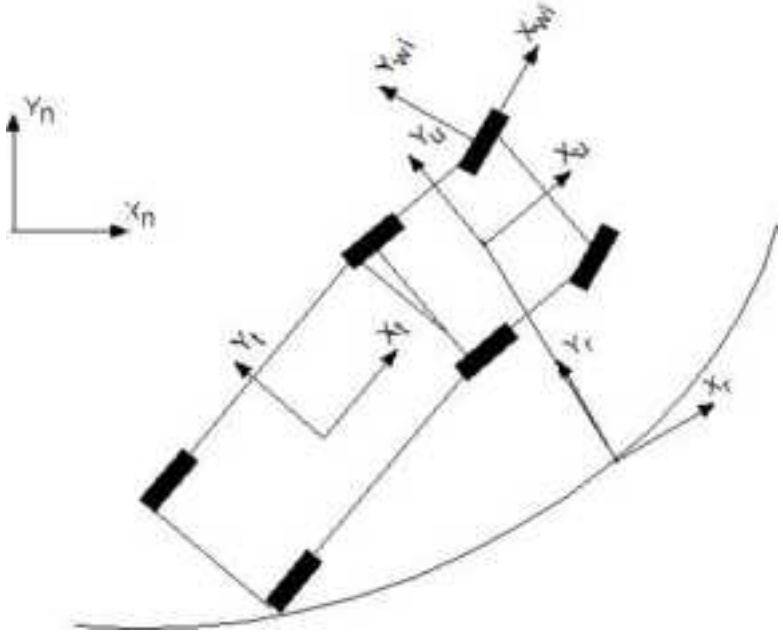

Fig. 2.3: Coordinate frames.

Table 2.2: Variables of interest

Variable	Description
x_n	Position of the tractor C.G. in the $\vec{i}_n$ direction of the inertial coordinate frame (X_n, Y_n)
y_n	Position of the tractor C.G. in the $\vec{j}_n$ direction of the inertial coordinate frame (X_n, Y_n)
x_r	Position of the tractor C.G. in the $\vec{i}_r$ direction of the road reference coordinate frame (X_r, Y_r)
y_r	Position of the tractor C.G. in the $\vec{j}_r$ direction of the road reference coordinate frame (X_r, Y_r)
e	Yaw angle of the tractor relative to the inertial coordinate frame (X_n, Y_n)
e_r	Yaw angle of the tractor relative to the road reference frame (X_r, Y_r)
e_f	Articulation angle of the trailer relative to the tractor coordinate frame (X_u, Y_u)
e_d	Yaw angle of the road relative to the inertial coordinate frame (X_n, Y_n)
V_x	Velocity of the tractor C.G. in the $\vec{i}_u$ direction of the tractor coordinate frame (X_u, Y_u)
V_y	Velocity of the tractor C.G. in the $\vec{j}_u$ direction of the tractor coordinate frame (X_u, Y_u)

The transformation from one coordinate system to another is considered a trivial task and thus it is not analyzed; however for purposes of thoroughness the transformation from the inertial to the tractor frame and vice-versa is provided below, just as an example:

$$\begin{bmatrix} \vec{i}_n \\ \vec{j}_n \end{bmatrix} = \begin{bmatrix} \cos e & -\sin e \\ \sin e & \cos e \end{bmatrix} \begin{bmatrix} \vec{i}_u \\ \vec{j}_u \end{bmatrix} \tag{2-1}$$

$$\begin{bmatrix} \vec{i}_u \\ \vec{j}_u \end{bmatrix} = \begin{bmatrix} \cos e & \sin e \\ -\sin e & \cos e \end{bmatrix} \begin{bmatrix} \vec{i}_n \\ \vec{j}_n \end{bmatrix} \tag{2-2}$$

Similar homogeneous transformations hold for all the other coordinate transformations.

Two kinematic equations that will be of use later in this chapter are the expressions of the tractor's and the trailer's velocity and acceleration in the inertial coordinate frame. To this end, it is observed that, by definition, the velocity vector of the tractors's C.G. is:

$$\begin{aligned} &\vec{V}_{cg1} = V_x \vec{i}_u + V_y \vec{j}_u \Rightarrow \\ &\vec{V}_{cg1} = \begin{bmatrix} V_x & V_y \end{bmatrix} \begin{bmatrix} \vec{i}_u \\ \vec{j}_u \end{bmatrix} \end{aligned} \tag{2-3}$$

Also it is clear that, by definition, the position vector of the tractor's C.G. is:

$$\begin{aligned} &\vec{r}_{cg1} = x_n \vec{i}_n + y_n \vec{j}_n \Rightarrow \\ &\dot{\vec{r}}_{cg1} = \vec{V}_{cg1} = \dot{x}_n \vec{i}_n + \dot{y}_n \vec{j}_n \Rightarrow \\ &\vec{V}_{cg1} = \begin{bmatrix} \dot{x}_n & \dot{y}_n \end{bmatrix} \begin{bmatrix} \vec{i}_n \\ \vec{j}_n \end{bmatrix} \end{aligned} \tag{2-4}$$

And since the inertial frame is stationary:

$$\begin{aligned} &\dot{\vec{r}}_{cg1} = \vec{V}_{cg1} = \dot{x}_n \vec{i}_n + \dot{y}_n \vec{j}_n \Rightarrow \\ &\vec{V}_{cg1} = \begin{bmatrix} \dot{x}_n & \dot{y}_n \end{bmatrix} \begin{bmatrix} \vec{i}_n \\ \vec{j}_n \end{bmatrix} \end{aligned} \tag{2-5}$$

Using Eq. (2-1), Eq. (2-5) becomes:

$$\begin{aligned} &\vec{V}_{cg1} = \begin{bmatrix} \dot{x}_n & \dot{y}_n \end{bmatrix} \begin{bmatrix} \cos e & -\sin e \\ \sin e & \cos e \end{bmatrix} \begin{bmatrix} \vec{i}_u \\ \vec{j}_u \end{bmatrix} \Rightarrow \\ &\vec{V}_{cg1} = \left(\dot{x}_n \cos e + \dot{y}_n \sin e \right) \vec{i}_u + \left(-\dot{x}_n \sin e + \dot{y}_n \cos e \right) \vec{j}_u \end{aligned} \tag{2-6}$$

Equating Eq. (2-3) and (2-6), yields:

$$V_x = \left(\dot{x}_n \cos e + \dot{y}_n \sin e \right) \tag{2-7}$$

$$V_y = \left(-\dot{x}_n \sin e + \dot{y}_n \cos e\right) \tag{2-8}$$

The tractor coordinate frame is fixed to the tractor so it is rotating about the vertical axis with rotational velocity $\dot{e}$, thus:

$$\begin{aligned} \dot{\vec{i}}_u &= \dot{e}\,\vec{j}_u \\ \dot{\vec{j}}_u &= -\dot{e}\,\vec{i}_u \end{aligned} \tag{2-9}$$

Therefore, differentiating Eq. (2-3) and using Eqs. (2-9), we obtain:

$$\begin{aligned} \dot{\vec{V}}_{cg1} &= \dot{V}_x \vec{i}_u + V_x \dot{\vec{i}}_u + \dot{V}_y \vec{j}_u + V_y \dot{\vec{j}}_u \Rightarrow \\ \dot{\vec{V}}_{cg1} &= \left(\dot{V}_x - V_y \dot{e}\right)\vec{i}_u + \left(\dot{V}_y + V_x \dot{e}\right)\vec{j}_u \end{aligned} \tag{2-10}$$

The inertial frame is stationary, so:

$$\dot{\vec{V}}_{cg1} = \ddot{x}_n \vec{i}_n + \ddot{y}_n \vec{j}_n \tag{2-11}$$

Using Eq. (2-1), Eq. (2-11) becomes:

$$\dot{\vec{V}}_{cg1} = \left(\ddot{x}_n \cos e + \ddot{y}_n \sin e\right)\vec{i}_u + \left(-\ddot{x}_n \sin e + \ddot{y}_n \cos e\right)\vec{j}_u \tag{2-12}$$

Hence, from Eq. (2-10) and (2-12), we obtain:

$$\left(\dot{V}_x - V_y \dot{e}\right) = \left(\ddot{x}_n \cos e + \ddot{y}_n \sin e\right) \tag{2-13a}$$

$$\left(\dot{V}_y + V_x \dot{e}\right) = \left(-\ddot{x}_n \sin e + \ddot{y}_n \cos e\right) \tag{2-14a}$$

By inverting the homogeneous transformation, we obtain:

$$\ddot{x}_n = \left(\dot{V}_x - V_y \dot{e}\right)\cos e - \left(\dot{V}_y + V_x \dot{e}\right)\sin e \tag{2-13b}$$

$$\ddot{y}_n = \left(\dot{V}_x - V_y \dot{e}\right)\sin e + \left(\dot{V}_y + V_x \dot{e}\right)\cos e \tag{2-14b}$$

As for the kinematics of the trailer, it is observed that the position vector of the trailer's C.G. is:

$$\begin{aligned} \vec{r}_{cg2} &= \vec{r}_{cg1} - d_1 \vec{i}_u - d_3 \vec{i}_t \Rightarrow \\ \dot{\vec{r}}_{cg2} &= \vec{V}_{cg2} = \dot{\vec{r}}_{cg1} - d_1 \dot{\vec{i}}_u - d_3 \dot{\vec{i}}_t \Rightarrow \\ \vec{V}_{cg2} &= \vec{V}_{cg1} - d_1 \dot{e}\,\vec{j}_u - d_3 \left(\dot{e} + \dot{e}_f\right)\vec{j}_t \end{aligned} \tag{2-15}$$

where we used the fact that the trailer's coordinate frame rotates with $\left(\dot{e} + \dot{e}_f\right)$. Taking into account Eq. (2-6) and the coordinate transformation from the trailer to the tractor coordinate frame, we obtain:

$$
\begin{aligned}
V_{cg2} &= \dot{x}_n \vec{i}_n + \dot{y}_n \vec{j}_n + d_1 \dot{e} \sin e \vec{i}_n - \cos e d_1 \dot{e} \vec{j}_n + \\
&+ \sin\left(e + e_f\right) d_3 \left(\dot{e} + \dot{e}_f\right) \vec{i}_n - \cos\left(e + e_f\right) d_3 \left(\dot{e} + \dot{e}_f\right) \vec{j}_n \\
&= \left(\dot{x}_n + d_1 \dot{e} \sin e + \sin\left(e + e_f\right) d_3 \left(\dot{e} + \dot{e}_f\right)\right) \vec{i}_n + \\
&\left(\dot{y}_n - \cos e d_1 \dot{e} - \cos\left(e + e_f\right) d_3 \left(\dot{e} + \dot{e}_f\right)\right) \vec{j}_n
\end{aligned} \tag{2-16}
$$

2.3 Road-tire Interaction

The study of the road-tire interaction is an extremely challenging matter since it involves the contact of two bodies (tire and road) accompanied by the following phenomena: tire rolling and slippage, tire viscoelastic deformation – especially of the contact patch – elastic (or sometimes plastic) deformation of the road and finally interference of debris such as dust, water, snow and ice. Another issue is the fact that the vertical load on the tire changes when the vehicle negotiates a turn, because of the weight transfer. Several complicated models based on analytical and experimental data have tried to capture the dynamics of the road-tire interaction. However, for nominal highway operation where road curvatures and longitudinal accelerations are small, it is universally accepted that a linear equation is sufficient to describe the tire forces.

Lateral Direction

In the lateral direction, the linear equation that yields the lateral tire force F_a is:

$$F_a = m\left(C_a a + C_g g\right) \tag{2-17}$$

where

- a is the slip angle defined as the angle between the velocity vector of the center of the wheel ($\vec{V}_{wi}$) and the orientation of the wheel (d is the orientation of the wheel in the coordinate frame of the associated unit, i.e. the tractor or trailer).
- *?* is the camber angle which was assumed 0 (see Section 2.1).
- C_a and $C_?$ is cornering and camber stiffness respectively. In general, both parameters increase as the tire pressure increases.

The lateral force will act in the lateral direction of each wheel as shown in the figure below.

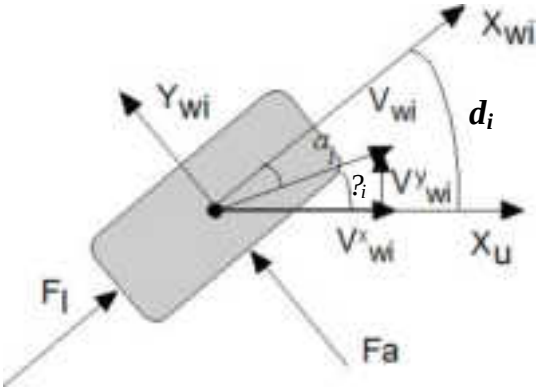

Fig. 2.4: The mechanics of the tire

For the *i*th wheel, Eq. (2-17) can be written as:

$$\vec{F}_a = mC_a\left(d_i - z_i\right)\vec{j}_{wi} \Rightarrow$$
$$\vec{F}_a = mC_a\left(d_i - \tan^{-1}\frac{V_{wi}{}^y}{V_{wi}{}^x}\right)\vec{j}_{wi} \tag{2-18}$$

Hence the calculation of the lateral force on each wheel boils down to the calculation of the wheel velocity vector V_{wi}. To this end, it is observed that the absolute position vector of each wheel is:

$$\vec{r}_{w1} = \vec{r}_{CG1} + l_1\vec{i}_u + \tfrac{1}{2}T_{w1}\vec{j}_u \tag{2-19}$$

$$\vec{r}_{w2} = \vec{r}_{CG1} + l_1\vec{i}_u - \tfrac{1}{2}T_{w1}\vec{j}_u \tag{2-20}$$

$$\vec{r}_{w3} = \vec{r}_{CG1} - l_2\vec{i}_u + \tfrac{1}{2}T_{w2}\vec{j}_u \tag{2-21}$$

$$\vec{r}_{w4} = \vec{r}_{CG1} - l_2\vec{i}_u - \tfrac{1}{2}T_{w2}\vec{j}_u \tag{2-22}$$

$$\vec{r}_{w5} = \vec{r}_{CG1} - d_1\vec{i}_u - l_3\vec{i}_t + \tfrac{1}{2}T_{w3}\vec{j}_t \Rightarrow$$
$$\vec{r}_{w5} = \vec{r}_{CG1} + \left(-l_3 - d_1\cos e_f\right)\vec{i}_t + \left(\tfrac{1}{2}T_{w3} - d_1\sin e_f\right)\vec{j}_t \tag{2-23}$$

$$\vec{r}_{w6} = \vec{r}_{CG1} - d_1\vec{i}_u - l_3\vec{i}_t - \tfrac{1}{2}T_{w3}\vec{j}_t \Rightarrow$$
$$\vec{r}_{w6} = \vec{r}_{CG1} + \left(-l_3 - d_1\cos e_f\right)\vec{i}_t + \left(-\tfrac{1}{2}T_{w3} - d_1\sin e_f\right)\vec{j} \tag{2-24}$$

Taking the derivative of Eqs. (2-19) to (2-24) gives the velocity of the center of wheel *i*.

$$\vec{V}_{w1} = \vec{V}_{CG1} + l_1\dot{\vec{i}}_u + \tfrac{1}{2}T_{w1}\dot{\vec{j}}_u \Rightarrow$$
$$\vec{V}_{w1} = \left(V_x - \tfrac{1}{2}T_{w1}\dot{e}\right)\vec{i}_u + \left(V_y + l_1\dot{e}\right)\vec{j}_u \tag{2-25}$$

$$\vec{V}_{w2} = \vec{V}_{CG1} + l_1\dot{\vec{i}}_u - \tfrac{1}{2}T_{w1}\dot{\vec{j}}_u \Rightarrow$$
$$\vec{V}_{w2} = \left(V_x + \tfrac{1}{2}T_{w1}\dot{e}\right)\vec{i}_u + \left(V_y + l_1\dot{e}\right)\vec{j}_u \tag{2-26}$$

$$\vec{V}_{w3} = \vec{V}_{CG1} - l_2\dot{\vec{i}}_u + \tfrac{1}{2}T_{w2}\dot{\vec{j}}_u \Rightarrow$$
$$\vec{V}_{w3} = \left(V_x - \tfrac{1}{2}T_{w2}\dot{e}\right)\vec{i}_u + \left(V_y - l_2\dot{e}\right)\vec{j}_u \qquad (2\text{-}27)$$

$$\vec{V}_{w4} = \vec{V}_{CG1} - l_2\dot{\vec{i}}_u - \tfrac{1}{2}T_{w2}\dot{\vec{j}}_u \Rightarrow$$
$$\vec{V}_{w4} = \left(V_x + \tfrac{1}{2}T_{w2}\dot{e}\right)\vec{i}_u + \left(V_y - l_2\dot{e}\right)\vec{j}_u \qquad (2\text{-}28)$$

$$\vec{V}_{w5} = \vec{V}_{CG1} + \left(-l_3 - d_1\cos e_f\right)\dot{\vec{i}}_t + \left(d_1\dot{e}_f\sin e_f\right)\vec{i}_t +$$
$$\left(-d_1\sin e_f + \tfrac{1}{2}T_{w3}\right)\dot{\vec{j}}_t + \left(-d_1\dot{e}_f\cos e_f\right)\vec{j}_t$$
$$\vec{V}_{w5} = \left(V_x\cos e_f + \left(V_y - d_1\dot{e}_1\right)\cos e_f - \tfrac{1}{2}T_{w3}\left(\dot{e} + \dot{e}_f\right)\right)\vec{i}_t +$$
$$+\left(-V_x\sin e_f + \left(V_y - d_1e_1\right)\cos e_f - l_3\left(\dot{e} + \dot{e}_f\right)\right)\vec{j}_t \qquad (2\text{-}29)$$

$$\vec{V}_{w6} = \vec{V}_{CG1} + \left(-l_3 - d_1\cos e_f\right)\dot{\vec{i}}_t + \left(d_1\dot{e}_f\sin e_f\right)\vec{i}_t +$$
$$\left(-d_1\sin e_f - \tfrac{1}{2}T_{w3}\right)\dot{\vec{j}}_t + \left(-d_1\dot{e}_f\cos e_f\right)\vec{j}_t$$
$$\vec{V}_{w6} = \left(V_x\cos e_f + \left(V_y - d_1\dot{e}_1\right)\cos e_f + \tfrac{1}{2}T_{w3}\left(\dot{e} + \dot{e}_f\right)\right)\vec{i}_t +$$
$$+\left(-V_x\sin e_f + \left(V_y - d_1e_1\right)\cos e_f - l_3\left(\dot{e} + \dot{e}_f\right)\right)\vec{j}_t \qquad (2\text{-}30)$$

The last two equations were transformed to the trailer coordinate frame, because this is the unit associated with the rear wheels. To conclude, the lateral forces are obtained as follows: First calculate ?*i*:

$$z_1 = \tan^{-1}\frac{\left(V_y + l_1\dot{e}\right)}{\left(V_x - \tfrac{1}{2}T_{w1}\dot{e}\right)} \qquad (2\text{-}31)$$

$$z_2 = \tan^{-1}\frac{\left(V_y + l_1\dot{e}\right)}{\left(V_x + \tfrac{1}{2}T_{w1}\dot{e}\right)} \qquad (2\text{-}32)$$

$$z_3 = \tan^{-1}\frac{\left(V_y - l_2\dot{e}\right)}{\left(V_x - \tfrac{1}{2}T_{w2}\dot{e}\right)} \qquad (2\text{-}33)$$

$$z_4 = \tan^{-1}\frac{\left(V_y - l_2\dot{e}\right)}{\left(V_x + \tfrac{1}{2}T_{w2}\dot{e}\right)} \qquad (2\text{-}34)$$

$$z_5 = \tan^{-1}\frac{\left(-V_x\sin e_f + \left(V_y - d_1\dot{e}_1\right)\cos e_f - l_3\left(\dot{e} + \dot{e}_f\right)\right)}{\left(V_x\cos e_f + \left(V_y - d_1\dot{e}_1\right)\cos e_f - \tfrac{1}{2}T_{w3}\left(\dot{e} + \dot{e}_f\right)\right)} \qquad (2\text{-}35)$$

$$z_6 = \tan^{-1}\frac{\left(-V_x\sin e_f + \left(V_y - d_1\dot{e}_1\right)\cos e_f - l_3\left(\dot{e} + \dot{e}_f\right)\right)}{\left(V_x\cos e_f + \left(V_y - d_1\dot{e}_1\right)\cos e_f + \tfrac{1}{2}T_{w3}\left(\dot{e} + \dot{e}_f\right)\right)} \qquad (2\text{-}36)$$

Recall the 5th assumption in the Section 2.1 which states that $d_i=0$ for $i=3,4,5,6$ (or any similar assumption that can be made) and calculate the slip angles:

$$a_i = d_i - z_i \tag{2-37}$$

Finally calculate the lateral forces relative to the tractor coordinate system:

$$\begin{aligned}
\vec{F}_{a1} &= C_{af} a_1 \vec{j}_{w1} = -C_{af} a_1 \sin(d_f)\vec{i}_u + C_{af} a_1 \cos(d_f)\vec{j}_u \\
\vec{F}_{a2} &= C_{af} a_2 \vec{j}_{w2} = -C_{af} a_2 \sin(d_f)\vec{i}_u + C_{af} a_2 \cos(d_f)\vec{j}_u \\
\vec{F}_{a3} &= C_{ar} a_3 \vec{j}_{w3} = C_{ar} a_3 \vec{j}_u \\
\vec{F}_{a4} &= C_{ar} a_4 \vec{j}_{w4} = C_{ar} a_4 \vec{j}_u \\
\vec{F}_{a5} &= C_{at} a_5 \vec{j}_{w5} = C_{at} a_5 \vec{j}_t = -C_{at} a_5 \sin(e_f)\vec{i}_u + C_{at} a_5 \cos(e_f)\vec{j}_u \\
\vec{F}_{a6} &= C_{at} a_6 \vec{j}_{w6} = C_{at} a_6 \vec{j}_t = -C_{at} a_6 \sin(e_f)\vec{i}_u + C_{at} a_6 \cos(e_f)\vec{j}_u
\end{aligned} \tag{2-38}$$

Longitudinal Direction

Similarly, in order to calculate the longitudinal tire force at each wheel, the longitudinal slip ratio is defined as:

$$\begin{aligned}
l_i &= \frac{w_{wi} r_{wi} - V_x}{V_x} \quad \textit{for braking} \\
l_i &= \frac{V_x - w_{wi} r_{wi}}{w_{wi} r_{wi}} \quad \textit{for traction,}
\end{aligned} \tag{2-39}$$

where $?_{wi}$ is the angular velocity of the ith tire. This longitudinal slip exists because the traction or braking force results in the tire deformation close to the contact patch. The longitudinal force acts in the longitudinal direction of each wheel, as shown in Fig. 2.4, and it is calculated by:

$$\begin{aligned}
\vec{F}_{l1} &= C_{lf} l_1 \vec{i}_{w1} = C_{lf} l_1 \cos(d_f)\vec{i}_u + C_{lf} l_1 \sin(d_f)\vec{j}_u \\
\vec{F}_{l2} &= C_{lf} l_2 \vec{i}_{w2} = -C_{lf} l_2 \cos(d_f)\vec{i}_u + C_{lf} l_2 \sin(d_f)\vec{j}_u \\
\vec{F}_{l3} &= C_{lr} l_3 \vec{i}_{w3} = C_{lr} l_3 \vec{i}_u \\
\vec{F}_{l4} &= C_{lr} l_4 \vec{i}_{w4} = C_{lr} l_4 \vec{i}_u \\
\vec{F}_{l5} &= C_{lt} l_5 \vec{i}_{w5} = C_{lt} l_5 \vec{i}_t = C_{lt} l_5 \cos(e_f)\vec{i}_u + C_{lt} l_5 \sin(e_f)\vec{j}_u \\
\vec{F}_{l6} &= C_{lt} l_6 \vec{i}_{w6} = C_{lt} l_6 \vec{i}_t = C_{lt} l_6 \cos(e_f)\vec{i}_u + C_{lt} l_6 \sin(e_f)\vec{j}_u
\end{aligned} \tag{2-40}$$

Clearly all the forces are now expressed in the tractor coordinate frame. If we want to transform them to the inertial coordinate frame we just use Eq. (2-2).

2.4 Equations of Motion

Model Relative to the Inertial Frame

First the equations of motion are derived relative to the inertial frame. The Lagrangian method is used, that is, the equations of motion result from the following equation:

$$\frac{d}{dt}\frac{\partial L}{\partial \dot{q}} - \frac{\partial L}{\partial q} = F_q \tag{2-41}$$

where L is the difference between the kinetic energy T and the potential energy V of the system, or $L=T-V$, q is the vector of independent variables and F is the generalized force vector.

The kinetic energy of the vehicle is the sum of the kinetic energy of the tractor and the trailer, that is:

$$T = \frac{1}{2}m_1 V_{cg1}^2 + \frac{1}{2}I_{z1}\dot{e}^2 + \frac{1}{2}m_2 V_{cg2}^2 + \frac{1}{2}I_{z2}\left(\dot{e}+\dot{e}_f\right)^2 \tag{2-42}$$

Recalling Eq. (2-5) and (2-16), the kinetic energy is:

$$\begin{aligned} T = {} & \frac{1}{2}m_1\dot{x}_n^2 + \frac{1}{2}m_1\dot{y}_n^2 + \frac{1}{2}I_{z1}\dot{e}^2 + \frac{1}{2}m_2\left(\dot{x}_n + d_1\dot{e}\sin e + \sin\left(e+e_f\right)d_3\left(\dot{e}+\dot{e}_f\right)\right)^2 + \\ & \frac{1}{2}m_2\left(\dot{y}_n - \cos e\, d_1\dot{e} - \cos\left(e+e_f\right)d_3\left(\dot{e}+\dot{e}_f\right)\right)^2 + \frac{1}{2}I_{z2}\left(\dot{e}+\dot{e}_f\right)^2 \end{aligned} \tag{2-43}$$

Since roll and pitch motions have been suppressed and the symmetry of the vehicle is assumed (Section 2.1), the potential energy does not change, thus the Lagrangian function is $L=T$. Applying the Lagrangian equation for the vector $q_n = \left[x_n \;\; y_n \;\; e \;\; e_f\right]^T$, the following results are obtained.

$$\begin{aligned} & \left(m_1+m_2\right)\ddot{x}_n + m_2 d_3 \sin\left(e+e_f\right)\left(\ddot{e}+\ddot{e}_f\right) + m_2 d_1 \ddot{e}\sin e + \\ & m_2 d_1 \dot{e}^2 \cos e + m_2 d_3 \cos\left(e+e_f\right)\left(\dot{e}+\dot{e}_f\right)^2 = F_{xn} \end{aligned} \tag{2-44}$$

$$\begin{aligned} & \left(m_1+m_2\right)\ddot{y}_n - m_2 d_3 \cos\left(e+e_f\right)\left(\ddot{e}+\ddot{e}_f\right) - m_2 d_1 \ddot{e}\cos e + \\ & m_2 d_1 \dot{e}^2 \sin e + m_2 d_3 \sin\left(e+e_f\right)\left(\dot{e}+\dot{e}_f\right)^2 = F_{yn} \end{aligned} \tag{2-45}$$

$$\begin{aligned} & \left(m_2 d_1 \sin e + m_2 d_3 \sin\left(e+e_f\right)\right)\ddot{x}_n + \left(-m_2 d_1 \cos e - m_2 d_3 \cos\left(e+e_f\right)\right)\ddot{y}_n + \\ & \left(I_{z1}+I_{z2}+m_2 d_1^2 + m_2 d_3^2 + 2m_2 d_1 d_3 \cos e_f\right)\ddot{e} + \left(I_{z2} + m_2 d_3^2 + m_2 d_1 d_3 \cos e_f\right)\ddot{e}_f - \\ & m_2 d_1 d_3 \dot{e}_f^2 \sin e_f - 2m_2 d_1 d_3 \dot{e}\dot{e}_f \sin e_f = F_e \end{aligned} \tag{2-46}$$

$$\begin{aligned} & \left(m_2 d_3 \sin\left(e+e_f\right)\right)\ddot{x}_n + \left(-m_2 d_3 \cos\left(e+e_f\right)\right)\ddot{y}_n + \\ & \left(I_{z2} + m_2 d_1^2 + m_2 d_3^2 + 2m_2 d_1 d_3 \cos e_f\right)\ddot{e} + \left(I_{z2} + m_2 d_3^2\right)\ddot{e}_f + \\ & m_2 d_1 d_3 \dot{e}^2 \sin e_f = F_{ef} \end{aligned} \tag{2-47}$$

where F_{xn}, F_{yn}, F_e and F_{ef} are the generalized forces corresponding to each generalized coordinate q_n. These forces can be calculated from Eq. (2-38) and (2-40), by transforming them to the inertial coordinate frame. Then F_{xn} is the sum of the forces projected to the X_n axis of the inertial coordinate system. Similarly, F_{yn} is the sum of the forces projected to the Y_n axis of the inertial coordinate system. A quick rule of thumb is that the generalized forces are the ones that produce work at the direction of the generalized coordinate.

This concludes the vehicle dynamics analysis of the nonlinear model of a two-unit vehicle. In the next subsections the equations of motion relative to the tractor coordinate frame and the road reference frame are presented.

Model Relative to the Tractor Frame

Multiplying Eq. (2-44) by *cose* and Eq. (2-45) by *sine*, adding them and taking into account Eq. (2-13a), yields:

$$\begin{aligned}&(m_1+m_2)\dot{V}_x+m_2d_3\sin e_f\left(\ddot{e}+\ddot{e}_f\right)-(m_1+m_2)V_y\dot{e}+\\&m_2d_1\dot{e}^2+m_2d_3\cos e_f\left(\dot{e}+\dot{e}_f\right)^2=F_{xn}\cos e+F_{yn}\sin e\end{aligned}\tag{2-48}$$

Similarly, multiplying Eq. (2-44) by -*sine* and Eq. (2-45) by *cose*, adding them and taking into account Eq. (2-14a), yields:

$$\begin{aligned}&(m_1+m_2)\dot{V}_y-m_2d_3\cos e_f\left(\ddot{e}+\ddot{e}_f\right)-m_2d_1\ddot{e}+(m_1+m_2)V_x\dot{e}+\\&+m_2d_3\sin e_f\left(\dot{e}+\dot{e}_f\right)^2=-F_{xn}\sin e+F_{yn}\cos e\end{aligned}\tag{2-49}$$

Also by substituting Eq. (2-13a) and (2-14) into Eq. (2-46), yields:

$$\begin{aligned}&-m_2d_1\dot{V}_y-m_2d_1V_x\dot{e}-m_2d_3\cos e_f\dot{V}_y-m_2d_3\cos e_fV_x\dot{e}+m_2d_3sine_f\dot{V}_x-m_2d_3sine_fV_y\dot{e}\\&\left(I_{z1}+I_{z2}+m_2d_1^2+m_2d_3^2+2m_2d_1d_3\cos e_f\right)\ddot{e}+\left(I_{z2}+m_2d_3^2+m_2d_1d_3\cos e_f\right)\ddot{e}_f-\\&m_2d_1d_3\dot{e}_f^2\sin e_f-2m_2d_1d_3\dot{e}\dot{e}_f\sin e_f=F_e\end{aligned}\tag{2-50}$$

Finally, Eq. (2.47) can be expressed in the tractor coordinate frame as follows:

$$\begin{aligned}&\left(-m_2d_3\dot{V}_y\cos e_f-m_2d_3V_x\dot{e}\cos e_f+m_2d_3\dot{V}_x\cos e_f-m_2d_3V_y\dot{e}\cos e_f\right)+\\&\left(I_{z2}+m_2d_3^2+m_2d_1d_3\cos e_f\right)\ddot{e}+\left(I_{z2}+m_2d_3^2\right)\ddot{e}_f+m_2d_1d_3\dot{e}^2\sin e_f=F_{ef}\end{aligned}\tag{2-51}$$

Hence the entire system is now expressed in the tractor coordinate frame. This representation is particularly useful when passenger comfort is of interest. It basically shows the state of the vehicle as viewed and felt from onboard.

Model Relative to Road Reference Frame

Finally a very useful model representation when lane following performance has to be validated, involves the expression of the vehicle states in terms of the road reference

coordinate frame. To this end, it is observed that the position vector of the the tractor's c.g. can be written as:

$$\vec{r}_{cg1} = \vec{r}_{Or} + x_r \vec{i}_r + y_r \vec{j}_r \Rightarrow \tag{2-52}$$

Where $\vec{r}_{Or}$ is the position vector of the origin of frame X_rY_r. From its definition, this frame travels at speed:

$$\dot{\vec{r}}_{Or} = \dot{x}_r \vec{i}_r \tag{2-53}$$

and since it follows the vehicle, it is clear that Eq. (2-52) can be written as:

$$\vec{r}_{cg1} = \vec{r}_{Or} + y_r \vec{j}_r \tag{2-54}$$

Differentiating Eq. (2-54), we obtain:

$$\begin{aligned} \dot{\vec{r}}_{cg1} &= \dot{\vec{r}}_{Or} + \dot{y}_r \vec{j}_r + y_r \dot{\vec{j}}_r \Rightarrow \\ \vec{V}_{cg1} &= \left(\dot{x}_r - y_r \dot{e}_d\right)\vec{i}_r + \dot{y}_r \vec{j}_r \end{aligned} \tag{2-55}$$

By the well known coordinate transformation, Eq. (2.55) becomes:

$$\vec{V}_{cg1} = \left(\left(\dot{x}_r - y_r \dot{e}_d\right)\cos e_r + \dot{y}_r \sin e_r\right)\vec{i}_u + \left(-\left(\dot{x}_r - y_r \dot{e}_d\right)\sin e_r + \dot{y}_r \cos e_r\right)\vec{j}_u \tag{2-56}$$

Comparing Eqs. (2-56) and (2-3), we obtain:

$$\begin{aligned} V_x &= \left(\dot{x}_r - y_r \dot{e}_d\right)\cos e_r + \dot{y}_r \sin e_r \\ V_y &= -\left(\dot{x}_r - y_r \dot{e}_d\right)\sin e_r + \dot{y}_r \cos e_r \end{aligned} \tag{2-57}$$

Using similar procedure the relationship between the accelerations in these two coordinate systems can be found. The next step is to visit Eqs. (2-48) – (2-51) and make the changes just like it was done with the conversion between the inertial frame and the tractor coordinate frame. Hence this step is not presented here.

2.5 Model Simplification for Control Design

The equations of motion derived above are non-linear, quite involved and they do not allow for any insight in terms of control design. Hence, it makes sense to make some more assumptions in order to bring the vehicle model to a more attractive form. To this end:

- The longitudinal velocity is considered constant, that is V_x=const and , $\dot{V}_x \approx 0$.
- The longitudinal tire force acting on the lateral tractor direction is negligible, $\vec{F}_{wi} = 0$ for i=1,2,…,6.
- The tire slip angles are the same on the left and right sides of the vehicle.

- The lateral tire force is linear, $\tan^{-1}(g) \approx g$.
- The articulation angle and rate, yaw rate, and the steering angle are small, $\sin(e_{f1}) \approx e_{f1}$ and $\cos(e_{f1}) \approx 1$, $\sin(d_{f1}) \approx d_{f1}$ and $\cos(d_{f1}) \approx 1$.
- Since the yaw rate, articulation angle and rate, and the steering angle are all small numerically, the higher order terms involving these variables are negligible.

These assumptions are all valid for nominal highway operation. Their influence on reducing the complexity of the model is discussed below. First of all, a close look at Eqs. (2-48) – (2-51) shows that Eq. (2.48), which describes the motion in the longitudinal direction, is now irrelevant so it can be omitted. Also the generalized forces are now much easier to find. More specifically the system becomes:

$$\begin{gathered}\left(m_1+m_2\right)\dot{V}_y - m_2 d_3 \cos e_f \left(\ddot{e}+\ddot{e}_f\right) - m_2 d_1 \ddot{e} + \left(m_1+m_2\right)V_x \dot{e} + \\ + m_2 d_3 \sin e_f \left(\dot{e}+\dot{e}_f\right)^2 = F_{a1}+F_{a2}+F_{a3}+F_{a4}+F_{a5}+F_{a6}\end{gathered} \tag{2-58}$$

$$\begin{gathered}-m_2 d_1 \dot{V}_y - m_2 d_1 V_x \dot{e} - m_2 d_3 \cos e_f \dot{V}_y - m_2 d_3 \cos e_f V_x \dot{e} - m_2 d_3 sin e_f V_y \dot{e} \\ \left(I_{z1}+I_{z2}+m_2 d_1^{\,2}+m_2 d_3^{\,2}+2m_2 d_1 d_3 \cos e_f\right)\ddot{e} + \left(I_{z2}+m_2 d_3^{\,2}+m_2 d_1 d_3 \cos e_f\right)\ddot{e}_f - \\ m_2 d_1 d_3 \dot{e}_f^{\,2} \sin e_f - 2m_2 d_1 d_3 \dot{e}\dot{e}_f \sin e_f = \\ = \left(F_{a1}+F_{a2}\right)l_1 - \left(F_{a3}+F_{a4}\right)l_2 - \left(F_{a5}+F_{a6}\right)\left(d_1 \cos e_f\right)\end{gathered} \tag{2-59}$$

$$\begin{gathered}\left(-m_2 d_3 \dot{V}_y \cos e_f - m_2 d_3 V_x \dot{e} \cos e_f - m_2 d_3 V_y \dot{e} \cos e_f\right) + \\ \left(I_{z2}+m_2 d_1^{\,2}+m_2 d_3^{\,2}+2m_2 d_1 d_3 \cos e_f\right)\ddot{e} + \left(I_{z2}+m_2 d_3^{\,2}\right)\ddot{e}_f + \\ m_2 d_1 d_3 \dot{e}^2 \sin e_f = \left(F_{a5}+F_{a6}\right)l_3\end{gathered} \tag{2-60}$$

where the tire slip angles are simplified as follows:

$$a_1 = a_2 = d - \frac{\left(V_y + l_1 \dot{e}\right)}{V_x} \tag{2-61}$$

$$a_3 = a_4 = -\frac{\left(V_y - l_2 \dot{e}\right)}{V_x} \tag{2-62}$$

$$a_5 = a_6 = e_f - \frac{\left(V_y - d_1 \dot{e}_1 - l_1\left(\dot{e}+\dot{e}_f\right)\right)}{V_x} \tag{2-63}$$

After some algebraic manipulations the system is brought to the following form:

$$M\ddot{q} + C\left(q,\dot{q}\right) + D\dot{q} + Kq = Fd_f \tag{2-64}$$

where:

$q = \left[\int V_y \quad e \quad e_f\right]^T$

$$M=\begin{bmatrix} m_1+m_2 & -m_2\left(d_1+d_3\cos e_f\right) & -m_2 d_3\cos e_f \\ -m_2\left(d_1+d_3\cos e_f\right) & I_{z1}+I_{z2}+m_2 d_1^{\,2}+m_2 d_3^{\,2}+2m_2 d_1 d_3\cos e_f & I_{z2}+m_2 d_3^{\,2}+m_2 d_1 d_3\cos e_f \\ -m_2 d_3\cos e_f & I_{z2}+m_2 d_3^{\,2}+m_2 d_1 d_3\cos e_f & I_{z2}+m_2 d_3^{\,2} \end{bmatrix}$$

$$C(q,\dot{q})=\begin{bmatrix} \left(m_1+m_2\right)V_x\dot{e}+m_2 d_3\sin e_f\left(\dot{e}+\dot{e}_f\right)^2 \\ -m_2\left(d_1+d_3\cos e_f\right)V_x\dot{e}-m_2 d_3\sin e_f V_y\dot{e}-2m_2 d_1 d_3\sin e_f\dot{e}\dot{e}_f-m_2 d_1 d_3\sin e_f\dot{e}_f^{\,2} \\ -m_2 d_3\sin e_f V_y\dot{e}-m_2 d_3\cos e_f V_x\dot{e}+m_2 d_1 d_3\sin e_f\dot{e}^2 \end{bmatrix}$$

$$D=\frac{2}{V_x}\begin{bmatrix} C_{af}+C_{ar}+C_{at} & l_1C_{af}-l_2C_{ar}-\left(l_3+d_1\right)C_{at} & -l_3C_{at} \\ l_1C_{af}-l_2C_{ar}-\left(l_3+d_1\right)C_{at} & l_1^{\,2}C_{af}+l_2^{\,2}C_{ar}+\left(l_3+d_1\right)^2C_{at} & l_3\left(l_3+d_1\right)C_{at} \\ -l_3C_{at} & l_3\left(l_3+d_1\right)C_{at} & l_3^{\,2}C_{at} \end{bmatrix}$$

$$K=\begin{bmatrix} 0 & 0 & -2C_{at} \\ 0 & 0 & 2\left(l_3+d_1\right)C_{at} \\ 0 & 0 & 2l_3C_{at} \end{bmatrix}$$

$$F=2C_{af}\begin{bmatrix} 1 & l_1 & 0 \end{bmatrix}^T$$

Using the sine and cosine approximations that were mentioned earlier and taking into account Eq. (2-57) and the relation between accelerations in the different frames, the dynamics of the system are expressed with respect to the road reference frame, as follows:

$$M_r\ddot{q}_r+C_r\dot{q}_r+K_rq_r=F_rd_f+E_1\dot{e}_d+E_2\ddot{e}_d \tag{2-65}$$

where:

$$q_r=\begin{bmatrix} y_r & e_r & e_f \end{bmatrix}^T$$

$$M=\begin{bmatrix} m_1+m_2 & -m_2\left(d_1+d_3\right) & -m_2 d_3 \\ -m_2\left(d_1+d_3\right) & I_{z1}+I_{z2}+m_2 d_1^{\,2}+m_2 d_3^{\,2}+2m_2 d_1 d_3 & I_{z2}+m_2 d_3^{\,2}+m_2 d_1 d_3 \\ -m_2 d_3 & I_{z2}+m_2 d_3^{\,2}+m_2 d_1 d_3 & I_{z2}+m_2 d_3^{\,2} \end{bmatrix}$$

$$C_r=\frac{2}{V_x}\begin{bmatrix} C_{af}+C_{ar}+C_{at} & l_1C_{af}-l_2C_{ar}-\left(l_3+d_1\right)C_{at} & -l_3C_{at} \\ l_1C_{af}-l_2C_{ar}-\left(l_3+d_1\right)C_{at} & l_1^{\,2}C_{af}+l_2^{\,2}C_{ar}+\left(l_3+d_1\right)^2C_{at} & l_3\left(l_3+d_1\right)C_{at} \\ -l_3C_{at} & l_3\left(l_3+d_1\right)C_{at} & l_3^{\,2}C_{at} \end{bmatrix}$$

$$K_r=\begin{bmatrix} 0 & -2\left(C_{af}+C_{ar}+C_{at}\right) & -2C_{at} \\ 0 & -2\left(l_1C_{af}-l_2C_{ar}-\left(l_3+d_1\right)C_{at}\right) & 2\left(l_3+d_1\right)C_{at} \\ 0 & 2l_3C_{at} & 2l_3C_{at} \end{bmatrix}$$

$$F = 2C_{af}\begin{bmatrix}1 & l_1 & 0\end{bmatrix}$$

$$E_1 = \begin{bmatrix} -(m_1+m_2)V_x - \frac{2}{V_x}\left(l_1C_{af} - l_2C_{ar} - (l_3+d_1)C_{at}\right) \\ m_2(d_1+d_3)V_x - \frac{2}{V_x}\left(l_1^2C_{af} + l_2^2C_{ar} + (l_3+d_1)^2C_{at}\right) \\ m_2d_3V_x - \frac{2}{V_x}l_3(l_3+d_1) \end{bmatrix}$$

$$E_2 = \begin{bmatrix} m_2(d_1+d_3) \\ -\left(I_{z1} + I_{z2}m_2(d_1+d_3)^2\right) \\ -\left(I_{z2} + m_2d_3^2m_2d_1d_3\right) \end{bmatrix}$$

The system can also be brought in the standard state space form as shown below:

$$\frac{d}{dt}\begin{bmatrix}q_r \\ \dot{q}_r\end{bmatrix} = \begin{bmatrix}0 & I \\ -M^{-1}K & -M^{-1}C\end{bmatrix}\begin{bmatrix}q_r \\ \dot{q}_r\end{bmatrix} + \begin{bmatrix}0 \\ M^{-1}F\end{bmatrix}d_f + \begin{bmatrix}0 \\ M^{-1}E_1\end{bmatrix}\dot{e}_d + \begin{bmatrix}0 \\ M^{-1}E_2\end{bmatrix}\ddot{e}_d \qquad (2\text{-}66)$$

$$\dot{x} = A\,x + B\,u + D$$

This is a very attractive form of the complex nonlinear model. It is purely linear time invariant, very simple, yet the fundamental lateral dynamic behavior remains very accurate [6].

2.6 Single Unit Vehicle modeling

One of the ways to derive the dynamic model of a single-unit vehicle, e.g. a passenger car, is to start modeling from scratch. The steps are going to be the same, but this time the model is simpler since there are less degrees of freedom.

On the other hand, a much faster way to create a model of such a vehicle is to derive it from the analysis above. More specifically, looking at Eq. (2-65), the third equation, which describes the trailer's motion relative to the tractor, has to be eliminated, since there is no trailer in single–unit vehicles. In the rest two equations, by setting all the variables and parameters relating to the trailer equal to 0, the following result is obtained.

$$M_r\ddot{q}_r + C_r\dot{q}_r + K_rq_r = F_rd_f + E_1\dot{e}_d + E_2\ddot{e}_d \qquad (2\text{-}67)$$

where:

$$q_r = \begin{bmatrix}y_r & e_r\end{bmatrix}^T$$

$$M = \begin{bmatrix}m_1 & 0 \\ 0 & I_{z1}\end{bmatrix}$$

$$C_r = \frac{2}{V_x}\begin{bmatrix} C_{af}+C_{ar} & l_1C_{af}-l_2C_{ar} \\ l_1C_{af}-l_2C_{ar} & l_1^2C_{af}+l_2^2C_{ar} \end{bmatrix}$$

$$K_r = \begin{bmatrix} 0 & -2\left(C_{af}+C_{ar}\right) \\ 0 & -2\left(l_1C_{af}-l_2C_{ar}\right) \end{bmatrix}$$

$$F = 2C_{af}\begin{bmatrix} 1 & l_1 \end{bmatrix}$$

$$E_1 = \begin{bmatrix} -m_1V_x - \frac{2}{V_x}\left(l_1C_{af}-l_2C_{ar}\right) \\ -\frac{2}{V_x}\left(l_1^2C_{af}+l_2^2C_{ar}\right) \end{bmatrix}$$

$$E_2 = \begin{bmatrix} m_2d_1 \\ -I_{z1} \end{bmatrix}$$

And again the system can be brought in the standard state space form as shown below:

$$\frac{d}{dt}\begin{bmatrix} q_r \\ \dot{q}_r \end{bmatrix} = \begin{bmatrix} 0 & I \\ -M^{-1}K & -M^{-1}C \end{bmatrix}\begin{bmatrix} q_r \\ \dot{q}_r \end{bmatrix} + \begin{bmatrix} 0 \\ M^{-1}F \end{bmatrix}d_f + \begin{bmatrix} 0 \\ M^{-1}E_1 \end{bmatrix}\dot{e}_d + \begin{bmatrix} 0 \\ M^{-1}E_2 \end{bmatrix}\ddot{e}_d \qquad (2\text{-}68)$$

$$\dot{x} \quad = \quad A \quad x \; + \quad B \quad u \; + \quad D$$

This is exactly the well known bicycle model that has been very widely used for control design for passenger vehicles. Notice that the system is considered a SISO LTI; the road curvature is viewed as a disturbance acting additively at the lateral acceleration of the vehicle. Comparing Eq. (2-65) and (2-67), it is clear that two-unit vehicles are much more complex, not only in terms of the number of parameters that affect dynamic behavior, but also in terms of structure (6 versus 4 states). Further details on the model and its dynamic behavior are presented in the next chapter.

3. LATERAL AUTONOMOUS FOLLOWING CONTROL DESIGN

As discussed earlier, lateral autonomous following is important in AHS, since it can act either as a backup system in case lane keeping techniques fail, or as a primary system if there is no road infrastructure to support lane keeping. The principle behind lateral autonomous following lies on the fact that by monitoring the relative lateral position of the preceding vehicle, it is possible to control the following vehicle.

However, the control design is a highly non-trivial task. As it is shown in the next section of this chapter, there are two important considerations that make control design challenging; first the plant itself, that is, the dynamic properties of the vehicle, present certain limitations and thus tradeoffs have to be made; secondly the fact that the controller relies on the preceding vehicle's position, instead of the fixed road, complicates the solution even more. Briefly speaking, this dependence introduces: (i) increased lateral errors due to rear-end off-tracking (the term is explained later) and (ii) platoon stability limitations due to the interconnection of the vehicles, as discussed in the Introduction.

The remainder of this chapter is organized as follows; first it is assumed that the following vehicle is monitoring the road centerline. This will unearth the limitations of automated lateral control design in general, that is, without the extra considerations arising from monitoring the preceding vehicle. Next, the control design will be altered to incorporate autonomous following systems, and more specifically to compensate for rear-end off-tracking. In addition, a mathematical analysis of platoon stability is presented and finally the solution to the problem and the final closed-loop system is developed. Again, the conclusions drawn for two-unit vehicles are applied to single-unit vehicles as well, therefore comparison is facilitated through the unified approach to the analysis of these two vehicle categories.

3.1 Conventional Autonomous Following Control Design

In the previous chapter, the general equations of motion for a single-unit and a two-unit vehicle were derived and simplified to a linear dynamic system, which was expressed in

the state-space form $\dot{x} = Ax + Bu$, see Eq. (2-66) and (2-68). Suppose that the controlled vehicle (vehicle 2) is following the *identical* preceding vehicle (vehicle 1). In order to determine its output equation it is assumed that a sensor is mounted at distance d_s from the vehicle's center of mass and monitors the relative distance of the rear end of the preceding vehicle, as shown in Fig. 3.1.

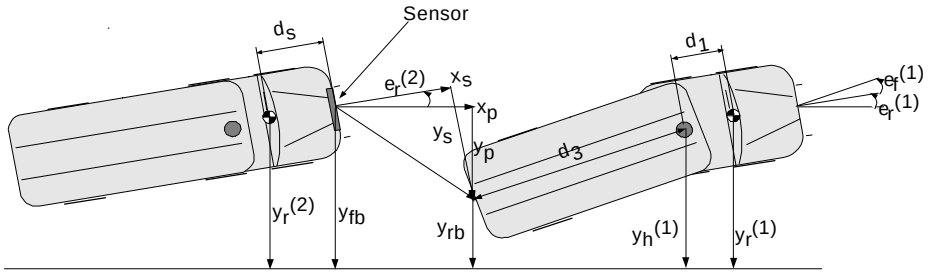

Fig. 3.1: System configuration for autonomous following.

The lateral distance measured by the sensor is $y_s{}^t$. Its relation to the vehicles' states is derived as follows:

$$\begin{aligned} y_s &= x_p \sin e_r^{(2)} + y_p \cos e_r^{(2)} \\ &= x_p \sin e_r^{(2)} + \left(y_{fb} - y_{rb} \right) \cos e_r^{(2)} \\ &= x_p \sin e_r^{(2)} + \left[\begin{array}{l} \left(y_r^{(2)} + d_s \sin e_r^{(2)} \right) - \\ \left(y_r^{(1)} - d_1 \sin e_r^{(1)} - d_3 \sin\left(e_r^{(1)} + e_f^{(1)} \right) \right) \end{array} \right] \cos e_r^{(2)} \end{aligned} \qquad (3\text{-}1)$$

Assuming that the angles $e_r^{(1)}, e_f^{(1)}$ and $e_r^{(2)}$ remain small, Eq. (3-1) is written:

$$y_s = \left(y_r^{(2)} - y_r^{(1)} \right) + \left(x_p + d_s \right) e_r^{(2)} + \left(\left(d_1 + d_3 \right) e_r^{(1)} + d_3 e_f^{(1)} \right) \qquad (3\text{-}2)$$

Similar analysis on single-unit vehicles yields:

$$y_s = \left(y_r^{(2)} - y_r^{(1)} \right) + \left(x_p + d_s \right) e_r^{(2)} + \left(d_{p1} e_r^{(1)} \right) \qquad (3\text{-}3)$$

where d_{p1} is the distance of the preceding vehicle's center of mass from its rear end. Both equations clearly show that the sensor measurement is composed of three terms: (i) the relative lateral position, (ii) the look-ahead term, that is, a quantity due to the fact that the preceding vehicle's rear end is at distance $\left(x_p + d_s \right)$ from the following vehicle's center of mass, and (iii) the off-tracking term. This last term describes the intuitive fact that the rear end of a vehicle does not necessarily follow the trajectory of the vehicle's center of

mass. For passenger vehicles this term is relatively small, while for tractor-semi-trailer vehicles trailer off-tracking makes control rather challenging. In this section, it is assumed that somehow the preceding vehicle manages to have its monitoring point exactly on the road centerline; thus rear end off-tracking is not present and so Eq. (3-3) becomes:

$$y_S = \left(y_r^{(2)} \right) + \left(x_p + d_s \right) e_r^{(2)} \tag{3-4}$$

Hence, in the general form, the output equation of a system that tracks the road centerline at some distance l_h ahead is given by:

$$y_S = \begin{bmatrix} 1 & l_h & 0 & 0 & 0 & 0 \end{bmatrix} \begin{bmatrix} y_r & e_r & e_f & \dot{y}_r & \dot{e}_r & \dot{e}_f \end{bmatrix}^T \quad for\ 2-unit\ vehicles \tag{3-5}$$

$$y_S = \begin{bmatrix} 1 & l_h & 0 & 0 \end{bmatrix} \begin{bmatrix} y_r & e_r & \dot{y}_r & \dot{e}_r \end{bmatrix}^T \quad for\ 1-unit\ vehicles \tag{3-6}$$

The set of Eqs. (3-5) and (2-66) constitute the linear plant for two-unit vehicles and the set of Eqs. (3-6) and (2-68) is the linear plant for single-unit vehicles. Taking the Laplace transform of the system yields the following block diagram for both cases:

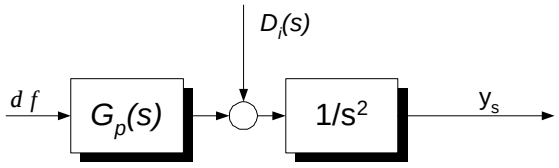

Fig. 3.2: The vehicle in its transfer function representation.

In Fig. 3.2, $G_p(s) = \frac{U(s)}{V(s)}$ is the transfer function from the steering angle *df* to the lateral acceleration $\ddot{y}_s$ and D_i is the road curvature disturbance. It is noted that $U(s)$ and $V(s)$ are different for single-unit and 2-unit vehicles.

It is interesting to see the frequency response of the $G_p(s)$ for various longitudinal velocities and look-ahead distances. For the parameters listed in Appendix A, the frequency response plots for single and two-unit vehicles are shown below. From these plots it is evident that for large longitudinal velocities, increased phase lag is present, and can be compensated for with large look-ahead distances. Clearly, there is a tradeoff between accuracy and ride comfort. Small look-ahead distances increase the accuracy but result in poorly damped zeros, that is oscillatory control, whereas large ones result in smoother control, but also in lane keeping inaccuracies. Also, from the comparison of the Bode plots, it is clear that two-unit vehicles (with the selected parameter values) are much more difficult to control at the same driving conditions.

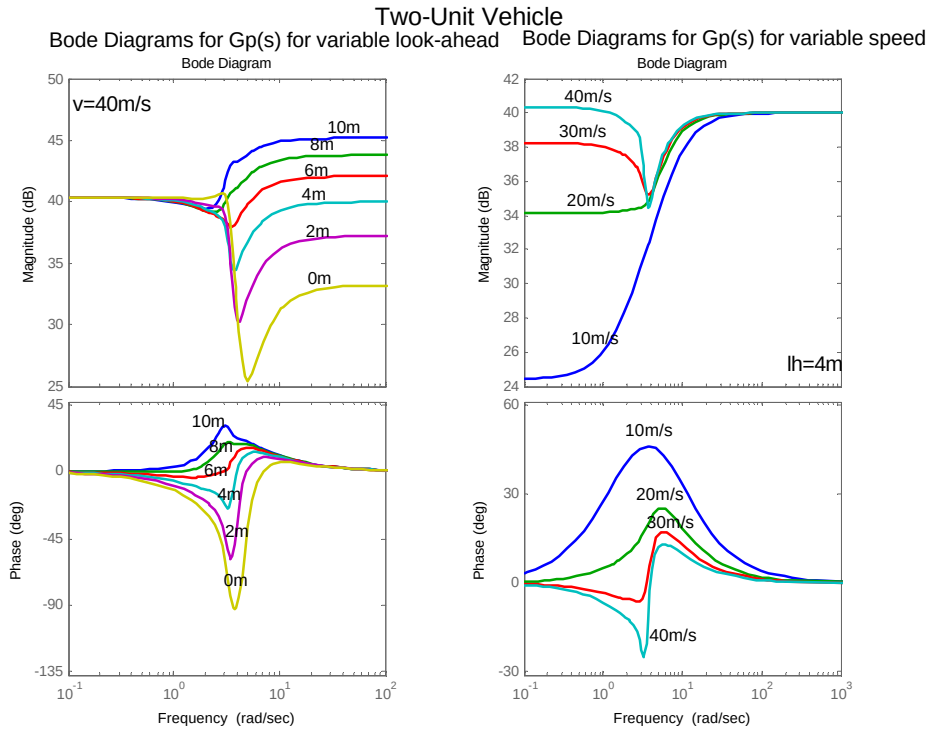

Fig. 3.3: Two-unit vehicle Bode diagrams.

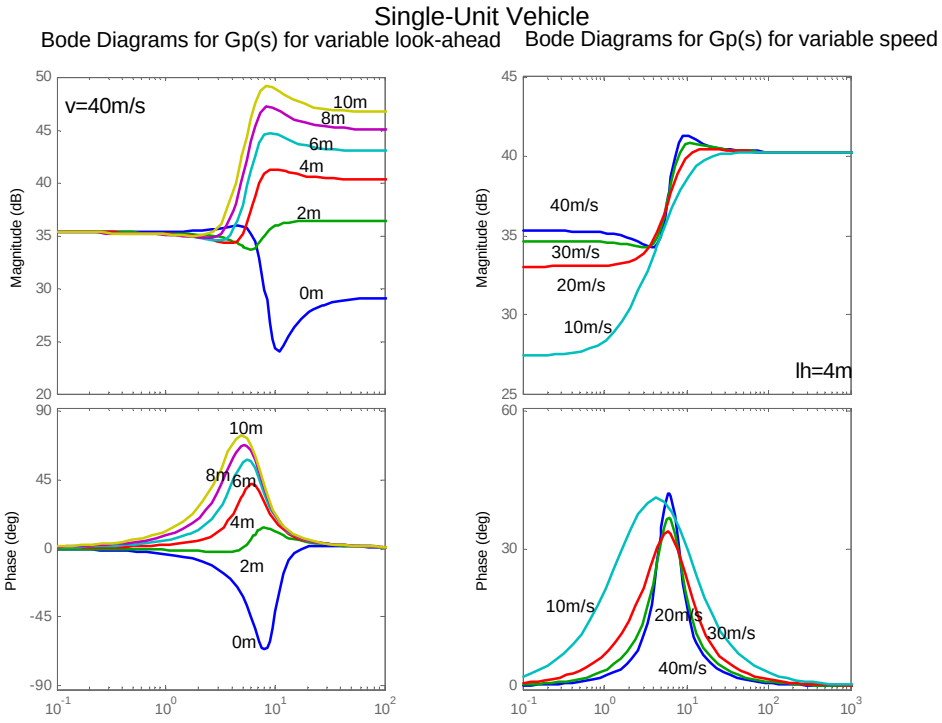

Fig. 3.4: Single-unit vehicle Bode diagrams.

The controller to be designed must attenuate the disturbances, achieve noise rejection and accurate tracking and finally have good performance for plant variations. In other words it has to be robust to plant uncertainties and especially to longitudinal velocity variations. In the figure below, the closed loop system along with the aforementioned disturbances is shown. As mentioned before, for the purposes of design, the quantity $\left(\left(d_1+d_3\right)e_r^{(1)}+d_3e_f^{(1)}-y_r^{(1)}\right)$ is assumed 0.

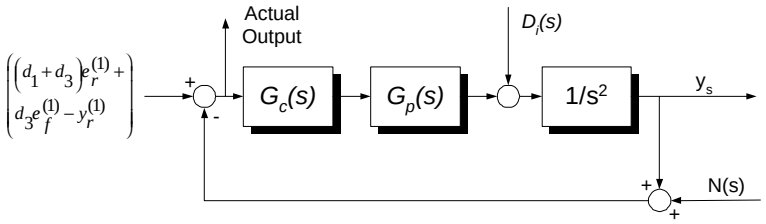

Fig. 3.5: Closed-loop system with disturbances.

Several controllers have been designed in the past. One of the most successful ones was a linear parameter-varying controller, that is, a controller whose parameters are continuous functions of the longitudinal velocity, [18]. Its downside is the very high computational power that is needed to implement such a controller. In this report, for simplicity reasons, a classical loop-shaping technique is selected. The major purpose of this report is not to come up with an optimal controller, but to show how nearly all controllers fail when the only information provided to them is the relative lateral error of the preceding vehicle's rear end. It is also intended to show that a simple lead lag controller, given the right information, can provide acceptable control without lateral error propagation along a platoon. Having said that, the controller proposed for a single-unit and two unit-vehicles with parameters close to those of the Appendix are shown below:

$$G_c^1(s)=\frac{0.262\ (s+1.356)\ (s+0.1528)}{(s+2.442)\ (s+0.1437)} \tag{3-7}$$

$$G_c^2(s)=\frac{108673(s+2.36)\ (s+0.81)}{(s+372.6)\ (s+97.47)\ (s+71.65)\ (s+0.853)} \tag{3-8}$$

The frequency response of the loop gains is shown below. It is noted that the nominal velocity was chosen to be *30m/s* for the single-unit vehicle and *25m/s* for the two-unit vehicle. The simulation results for a simple curvature profile are shown in the next figure.

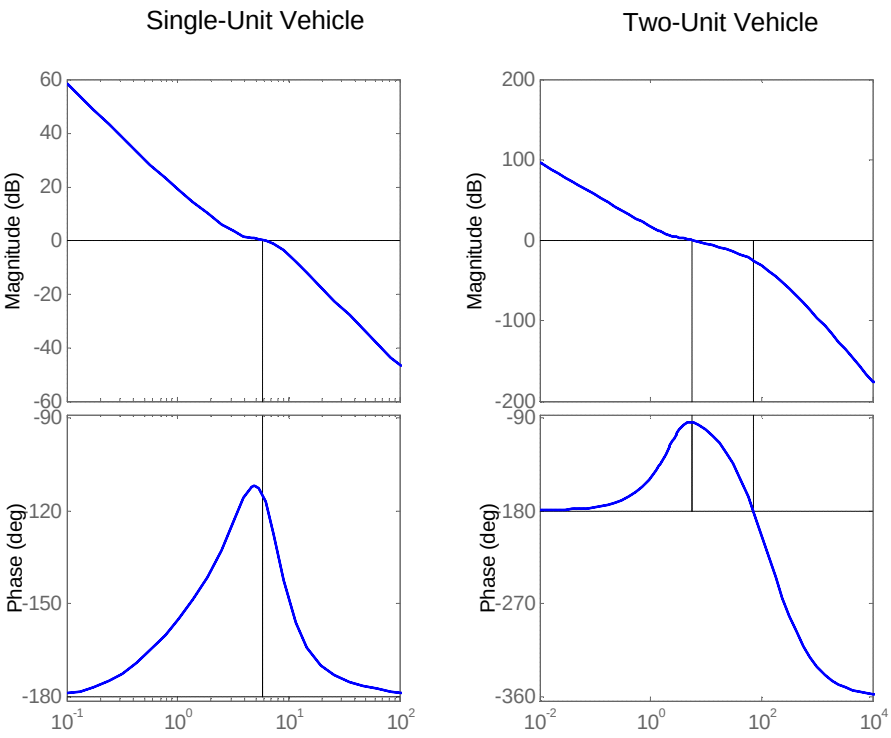

Fig. 3.6: Loop gain frequency responses for both types of vehicles.

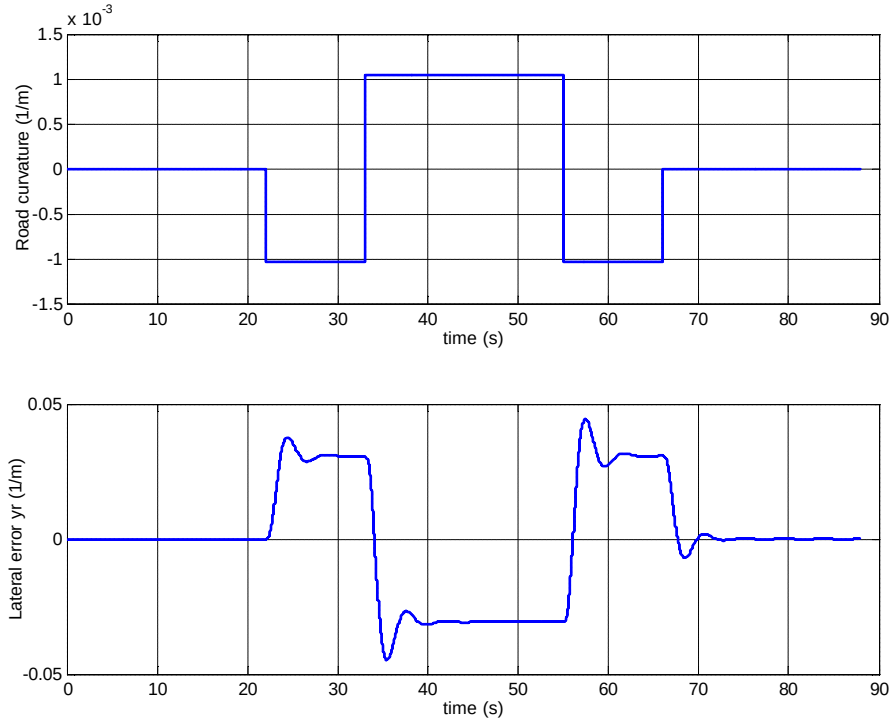

Fig. 3.7: Two-unit vehicle negotiating a curvature profile.

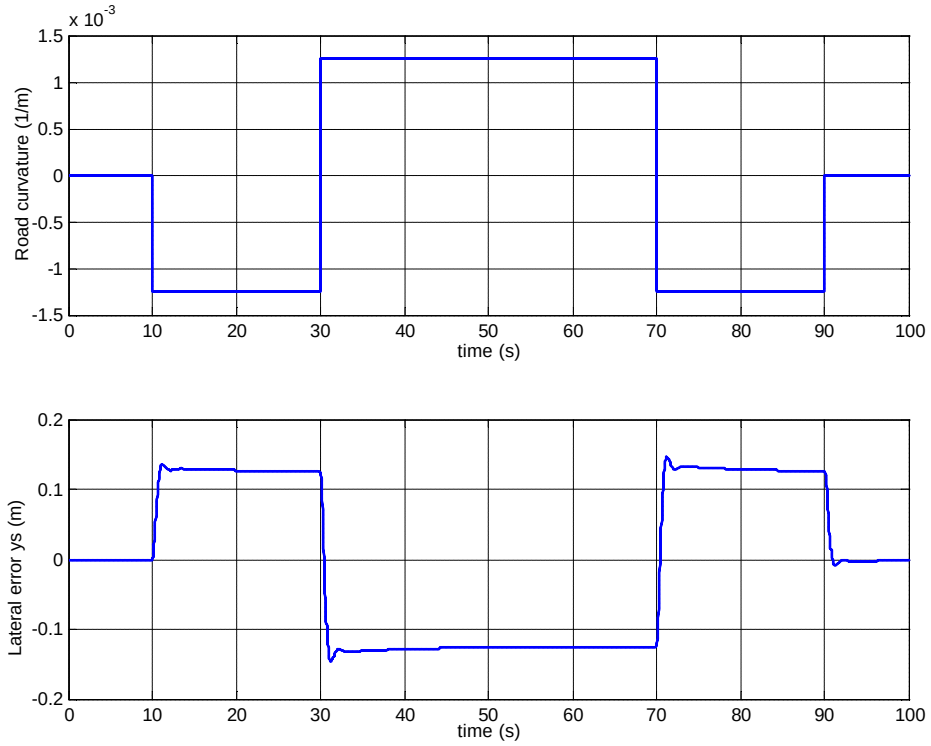

Fig. 3.8: Single-unit vehicle negotiating a curvature profile.

Clearly, both systems present good robustness properties (high gain and phase margins). In addition, in terms of time domain response, the simulation results show acceptable performance, since lane keeping remains within satisfactory limits.

Although, the designed controllers behave acceptably in terms of lane keeping, when it comes to implementing platooning through autonomous following, the system proves to be completely inadequate. The figure below shows the simulation results of a platoon of 3 passenger vehicles, each implementing autonomous following by monitoring the preceding vehicle's rear end and using the controller described in Eq. (3-7). The lateral error propagates along the platoon, indicating the absence of lateral platoon stability. Similar non-acceptable results are obtained for two-unit vehicles as well. In both simulations the parameters used were taken from Appendix A.

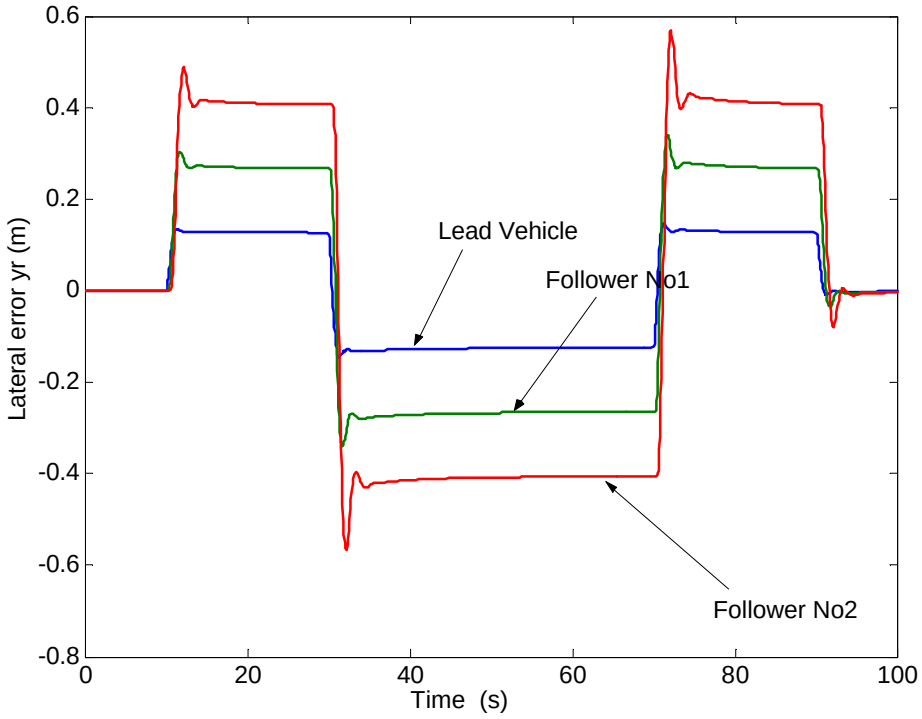

Fig. 3.9: Platoon of three single-unit vehicles negotiating a curvature profile.

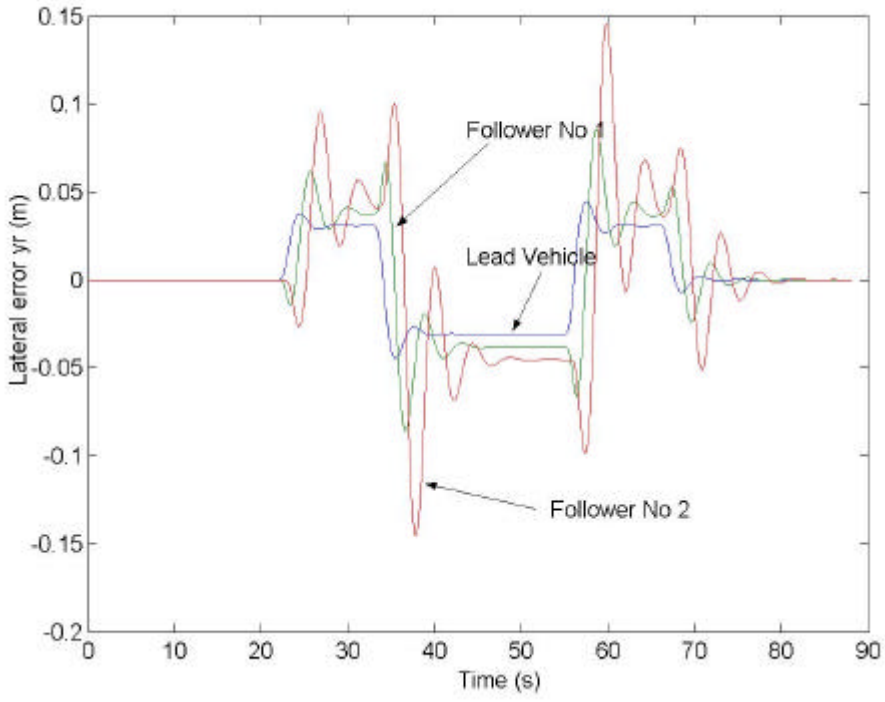

Fig. 3.10: Platoon of three two-unit vehicles negotiating a curvature profile.

Therefore, it is concluded that this simple method of autonomous following is not adequate for platooning, especially when the platoon size is large. The insufficiency of the control design presented above motivates for the development of a new controller, which is analyzed in the next section.

3.2. Autonomous Following Control Design with Off-tracking Compensation

One would suspect that the simplifying assumption that the preceding vehicle manages to have its monitoring point exactly on the road centerline is not valid. Indeed, the offset created by rear end off-tracking is too large to be neglected and there is also the $y_r^{(1)}$ term which represents the inherent interconnection between the two vehicles. Especially for tractor-semi-trailers, trailer off-tracking is quite large due to the significant length of the trailer. Hence, it has to be compensated for.

One way to compensate for the rear end off-tracking term, is to have the sensor track the preceding vehicle's center of mass instead of its rear end. This requires the installation of a reflective surface on the plane, which the preceding vehicle's center of mass lies on, e.g. on the roof. Clearly, this approach raises practical implementation issues, but if it is implemented, then according to Fig. 3.1, the look-ahead distance increases and the sensor output, becomes:

$$y_s = \left(y_r^{(2)} - y_r^{(1)}\right) + \left(x_p' + d_s\right)e_r^{(2)} \tag{3-9}$$

where x_p' is now the distance between the sensor and the measured point. Alternatively, it is possible to measure the relative yaw angle $\left(e_r^{(2)} - e_r^{(1)} - e_f^{(1)}\right)$ by scanning two points on the rear end of the preceding vehicle and using simple kinematic equations. Then, by adding in Eq. (3-2) the term $d_3\left(e_r^{(2)} - e_r^{(1)} - e_f^{(1)}\right)$, the output becomes:

$$\begin{aligned}
y_s &= \left(y_r^{(2)} - y_r^{(1)}\right) + \left(x_p + d_s\right)e_r^{(2)} + \left(\left(d_1 + d_3\right)e_r^{(1)} + d_3 e_f^{(1)}\right) + d_3\left(e_r^{(2)} - e_r^{(1)} - e_f^{(1)}\right) \Rightarrow \\
y_s &= \left(y_h^{(2)} + d_1 e_r^{(2)} - y_h^{(1)} - d_1 e_r^{(1)}\right) + \left(x_p + d_s\right)e_r^{(2)} + \\
&\quad \left(\left(d_1 + d_3\right)e_r^{(1)} + d_3 e_f^{(1)}\right) + d_3\left(e_r^{(2)} - e_r^{(1)} - e_f^{(1)}\right) \Rightarrow \\
y_s &= \left(y_h^{(2)} - y_h^{(1)}\right) + \left(x_p + d_s + d_1 + d_3\right)e_r^{(2)}
\end{aligned} \tag{3-10}$$

Thus, the control points are no longer the centers of mass, but the hitches of the heavy vehicles. In order to avoid this change of control point, the relative yaw angle $\left(e_r^{(2)} - e_r^{(1)} - e_f^{(1)}\right)$ is multiplied by $\left(d_1 + d_3\right)$ and, at the same time, the preceding vehicle's

articulation angle $e_f^{(1)}$ is communicated and multiplied by d_1. Adding the output of the monitoring device with these two quantities yields:

$$\begin{aligned} y_s &= \left(y_r^{(2)} - y_r^{(1)}\right) + \left(x_p + d_s\right)e_r^{(2)} + \left(\left(d_1 + d_3\right)e_r^{(1)} + d_3 e_f^{(1)}\right) + \\ &\quad \left(d_1 + d_3\right)\left(e_r^{(2)} - e_r^{(1)} - e_f^{(1)}\right) + d_1 e_f^{(1)} \Rightarrow \\ y_s &= \left(y_r^{(2)} - y_r^{(1)}\right) + \left(x_p + d_s + d_1 + d_3\right)e_r^{(2)} \end{aligned} \qquad (3\text{-}11)$$

It is clear that this new input to the controller eliminates trailer off-tracking, but it requires the installation of an inter-vehicle communication system. If this is not possible, it is recommended that the controlled vehicle use its own articulation angle measurements as the best estimate of $e_f^{(1)}$.

Similar analysis for single-unit vehicles transforms Eq. (3-3) to Eq. (3-12). In this case of course inter-vehicle communication is not needed since single-unit vehicles do not have an articulation point.

$$y_s = \left(y_r^{(2)} - y_r^{(1)}\right) + \left(x_p + d_s + d_{p1}\right)e_r^{(2)} \qquad (3\text{-}12)$$

From the analysis above, it is evident that the off-tracking term and hence the bias that it introduces is eliminated. The downside of this method is that relative yaw angles are usually very small during highway operation; hence the sensor resolution has to be high enough to yield reliable measurements. The simulation results for this new closed loop system are shown below for both single-unit and two-unit vehicles

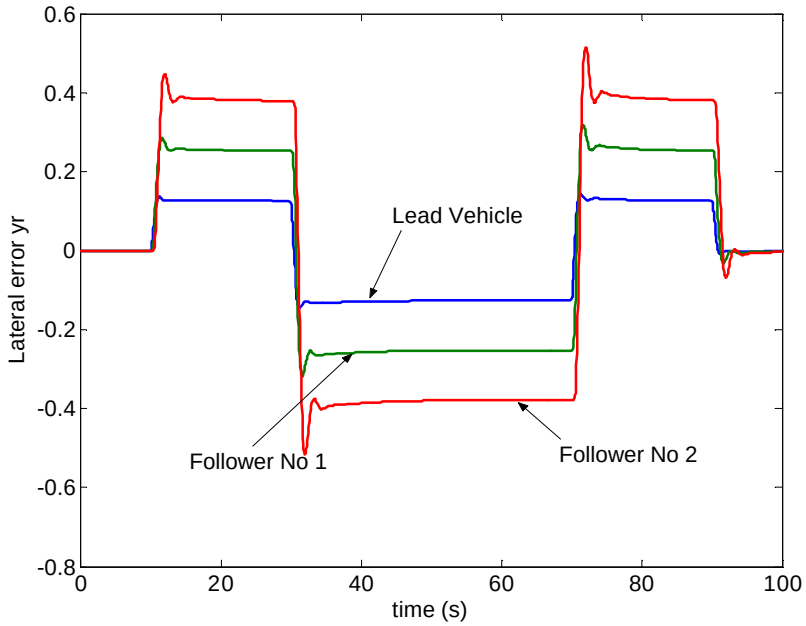

Fig. 3.11: Platoon of three single-unit vehicles with off-tracking compensation.

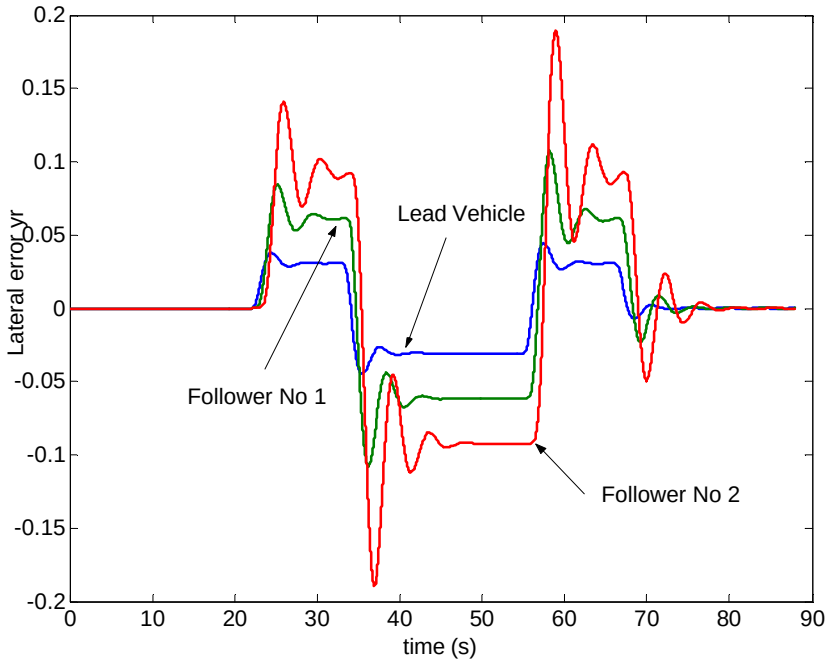

Fig. 3.12: Platoon of three two-unit vehicles with off-tracking compensation.

As expected, the lateral error propagation still exists but it is smaller this time for the single-unit vehicle case. As for the two-unit vehicle platoon, it is clear that although the initial error is a bit larger, it stable converges to a steady state error whereas without off-tracking compensation the error did not settle and was unpredictable.

Finally, it is possible to reduce or even eliminate the look-ahead term by storing the sensor measurements, translating and rotating them according to the motion of the vehicle and using them in the control law when the longitudinal distance between the control points (either centers of mass or hitches) takes the desire look-ahead value. Specifically, for known yaw rate, the sensor measurement is manipulated at each time step as follows:

$$x_{traj}[k]=\left(-e_r^{(1)}y_{traj}[k-1]-V_x\right)\Delta t+x_{traj}[k-1] \tag{3-13}$$

$$y_{traj}[k]=\left(e_r^{(1)}x_{traj}[k-1]-V_y\right)\Delta t+y_{traj}[k-1] \tag{3-14}$$

where $\dot{x}$ and $\dot{y}$ is the longitudinal and lateral velocity at the vehicle's reference frame respectively. When the longitudinal distance between the control points becomes zero, then the output of the system becomes:

$$y_s=y_r^{(2)}-y_r^{(1)} \tag{3-15}$$

Essentially, this version implements a look-down scheme, which has two problems:

(i) it requires the yaw rate of the vehicle, which means that one more sensor has to be installed. Normally, yaw rate is measured by a yaw rate gyrometer; however, this sensor often presents some drifting properties along time, rendering its measurements inaccurate.

(ii) As seen from the open-loop body plots the look-down scheme gives quite oscillatory control due to the poorly damped zeros that occur when the look-ahead distance approaches *0*.

3.3 The Notion of Lateral Platoon Stability

In the previous section, it was shown that the lateral error propagates along the platoon of vehicles, even when rear end off-tracking compensation is used. The reason behind this error propagation is the fact that each vehicle controller relies on measurements of the position relative to that of the preceding vehicle rather than its absolute position. This interconnection prompts for a mathematical analysis of platoon stability.

Definition: A group of n vehicles is laterally platoon stable in the l_p sense if $\forall i \in [2,n] \quad \left\| y_r^{(i)}(t) \right\|_p < \left\| y_r^{(i-1)}(t) \right\|_p$.

where $y_r^{(i-1)}(t)$ and $y_r^{(i)}(t)$ is the lateral error of the *(i-1)*th and *i*th vehicle relative to the road reference frame respectively. Since we are concerned about the lateral error propagation, we deal with l_∞ stability. Hence, the lateral platoon stability condition is:

$$\max_t \left| y_r^{(i)}(t) \right| < \max_t \left| y_r^{(i-1)}(t) \right| \tag{3-15}$$

For linear systems, the above condition implies that lateral l_∞ platoon stability is achieved when (i) the following equation holds:

$$\left\| \frac{Y_r^{(i)}(jw)}{Y_r^{(i-1)}(jw)} \right\|_\infty < 1 \Rightarrow \left| \frac{Y_r^{(i)}(jw)}{Y_r^{(i-1)}(jw)} \right| < 1, \quad \forall w \tag{3-16}$$

AND (ii) the impulse response of the transfer function from $Y_r^{(i-1)}$ to $Y_r^{(i)}$ does not change sign. Conversely, a platoon is laterally platoon unstable when there exists w such that:

$$\left\| \frac{Y_r^{(i)}(jw)}{Y_r^{(i-1)}(jw)} \right\|_\infty > 1 \tag{3-17}$$

Reformulating the problem of the autonomous following scheme and assuming that rear end off-tracking has been compensated for, the block diagram that describes the interconnection between the *i*th and the *(i-1)*th vehicle is shown in the figure below, and the transfer function is described by Eq. (3-18).

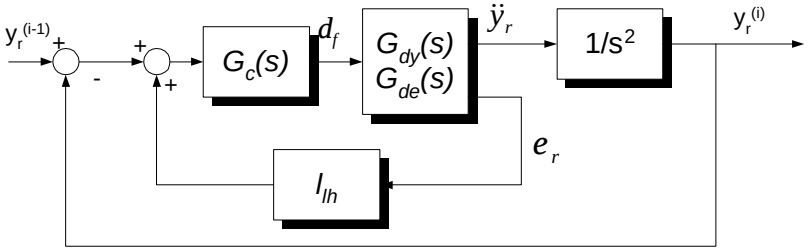

Fig. 3.13: Block diagram for the interconnection between *i*th and *(i-1)*th vehicle.

$$\frac{Y_r^{(i)}(s)}{Y_r^{(i-1)}(s)} = \frac{s^{-2}G_{pc}(s)}{1+s^{-2}G_{pc}(s)} \tag{3-18}$$

where $G_{pc}(s) = \frac{G_{dy}(s)G_c(s)}{1+l_{lh}G_{de}(s)G_c(s)}$ and l_{lh} is the look-ahead distance. It is clear that for $l_{lh}=0$, the system corresponds to the look-down scheme. Representing the loop gain as a complex number, that is:

$$L(jw) = (wj)^{-2}G_{pc}(jw) = r_L(jw)\cdot e^{jf(jw)} \tag{3-19}$$

then Eq. (3-16) becomes:

$$\left|\frac{r_L(jw)\cdot e^{jf(jw)}}{1+r_L(jw)\cdot e^{jf(jw)}}\right| < 1 \Rightarrow$$

$$\frac{r_L(jw)}{\sqrt{1+r_L^{\,2}(jw)+2r_L(jw)\cos f}} < 1 \Rightarrow$$

$$r_L(jw)\cos f > -0.5 \Rightarrow$$

$$\mathrm{Re}\{r_L(jw)\} > -0.5 \tag{3-20}$$

This means that the first condition for lateral platoon stability in the l_∞ sense is satisfied if the open-loop Nyquist plot lies on the right of the line $x=-0.5\ \forall w$. This is a very important conclusion, since it is a fast criterion to determine if the platoon is unstable. It should be stressed again that it does not guarantee platoon stability since it does not give any information about the impulse response of the transfer function. Several

simulations showed that it is possible to achieve lateral platoon stability by merely measuring the relative distance between the preceding and the following vehicle. In practice, if the look-ahead distance is small the controller gain has to be very small as well to satisfy the stability condition. Conversely, for larger controller gains platoon stability is achieved when the look-ahead distance is increased. In the first case, the result is slow transients resulting in poor performance, while in the second case vehicles cut the corners of the turns that they negotiate. Thus, lateral platoon stability and satisfactory performance is practically impossible to achieve simultaneously. What can be guaranteed is prevention of lateral error propagation for a certain frequency band. The following example illustrates such a case.

Example

For the tractor-semi-trailer vehicle parameters and the controller used in the previous section with zero look-ahead distance, the open-loop Nyquist plot is shown in Fig 3.14.

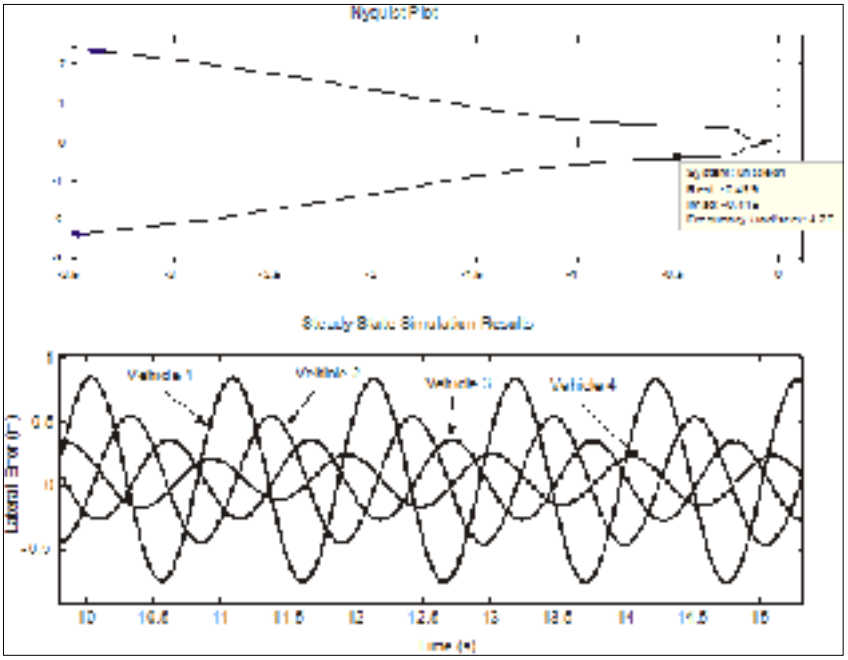

Fig. 3.14: Open loop Nyquist plot of the tractor-semi-trailer system (a), and simulation of a 4-vehicle platoon, (b).

From this figure, it can be concluded that a platoon consisting of the exact same vehicles is laterally unstable since the Nyquist plot does not lie on the right of the line $x=-0.5$. Fig. 3.14b shows the steady state simulation results for a 4-vehicle platoon whose lead vehicle oscillates at a frequency of *6rad/s*. It is evident that, although this is not a realistic highway curvature profile, there is no error propagation.

3.4 Adding Inter-Vehicle Communication

No Communication Delay

In order to obtain platoon stability without compromising performance, one can either redesign the interconnected system so that the lateral platoon stability criterion is satisfied, or eliminate the interconnection of the vehicles. In the latter case, if the reference trajectory for each vehicle is not that of its preceding vehicle but all vehicles share the same reference trajectory, then each vehicle tries to follow this trajectory independent of the motion of the other vehicles and thus the platoon is no longer a string of vehicles. Hence, platoon stability analysis as conducted previously is no longer valid. The platoon is stable as long as a stabilizing controller is designed for each vehicle.

In order to achieve vehicle "disconnection" without the need of road infrastructure, the addition of inter-vehicle communication is studied. Ideally, an accurate Global Positioning System (GPS) installed on the lead-vehicle and the transmission of its position to the platoon would be sufficient to achieve a common reference trajectory for all vehicles. However, there are several deployment issues with this solution such as guaranteeing fast real-time information from the GPS. Thus, making use of the existing on-board sensors seems a wise solution.

Assume a platoon of *n* identical vehicles, and the *i*th vehicle to be the vehicle of interest. Recall that each vehicle can measure three quantities:

(i) Relative lateral position $m_1^{(i)} = \left(y_r^{(i)} - y_r^{(i-1)} \right) + \left(x_p + d_s \right) e_r^{(i)} + \left(\left(d_1 + d_3 \right) e_r^{(i-1)} + d_3 e_f^{(i-1)} \right)$

(ii) Relative yaw $m_2^{(i)} = \left(e_r^{(i)} - e_r^{(i-1)} - e_f^{(i-1)} \right)$

(iii) Articulation angle $m_3^{(i)} = e_f^{(i)}$

where $y_r^{(0)}$ $e_r^{(0)}$ and $e_f^{(0)}$ are assumed 0. This essentially says that the lead vehicle knows its position relative to the road centerline. At each time instant *t*, the *i*th vehicle measures these quantities $m_1^{(i)}, m_2^{(i)}, m_3^{(i)}$, receives the measurements of all the preceding vehicles $m_1^{(k)}, m_2^{(k)}, m_3^{(k)}$, *k=1,2,..i-1* and algebraically manipulates them as follows:

$$y_{s1}^{(i)}\{t\} = \sum_{k=1}^{i} m_1^{(k)}\{t\} - \left(x_p + d_s + d_1 + d_3 \right) \sum_{k=1}^{i-1} (i-k) m_2^{(k)}\{t\} - \sum_{k=1}^{i-1} \left[\left(x_p + d_s + d_1 + d_3 \right)(i-k) - d_3 \right] m_3^{(k)}\{t\} \tag{3-21}$$

The result of Eq. (3-21) is:

$$y_s^{(i)}\{t\} = y_r^{(i)}\{t\} + \left(x_p + d_s\right) e_r^{(i)}\{t\} \tag{3-22}$$

This it the new output equation or else the input to the controller. It clearly shows that the vehicles have been "disconnected", in the sense that the controller input of each vehicle - and thus its output - does not rely on the position of the preceding vehicles. It basically reconstructs the road centerline position from the relative errors of the preceding vehicles.

For single-unit vehicles we have $m_1^{(i)} = \left(y_r^{(i)} - y_r^{(i-1)}\right) + \left(x_p + d_s\right) e_r^{(i)} + \left(\left(d_{p1}\right) e_r^{(i-1)}\right)$, and $m_2^{(i)} = \left(e_r^{(i)} - e_r^{(i-1)}\right)$. The input to the controller should now be:

$$y_{s1}^{(i)}\{t\} = \sum_{k=1}^{i} m_1^{(k)}\{t\} - \left(x_p + d_s + d_{p1}\right) \sum_{k=1}^{i-1} (i-k)\, m_2^{(k)}\{t\} \tag{3-23}$$

and the result is:

$$y_s^{(i)}\{t\} = y_r^{(i)}\{t\} + \left(x_p + d_s\right) e_r^{(i)}\{t\} \tag{3-24}$$

This scenario is simulated for both single-unit and two-unit vehicles and the results are shown below. To facilitate understanding the response around the 10th second has been blown up.

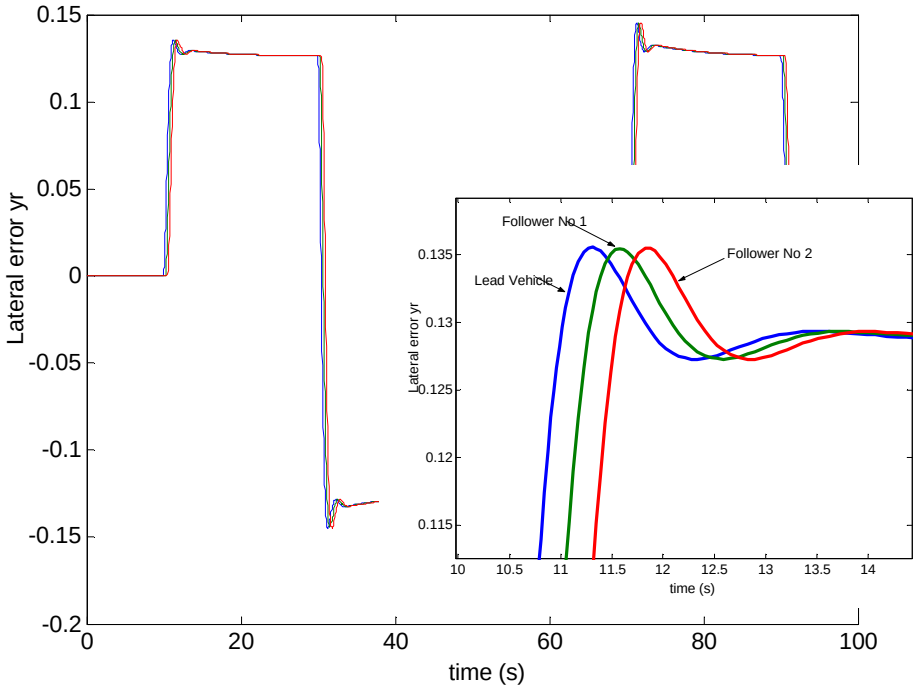

Fig. 3.15: Simulation of single-unit vehicle platoon w/ ideal inter-vehicle communication (entire simulation and blown-up detail).

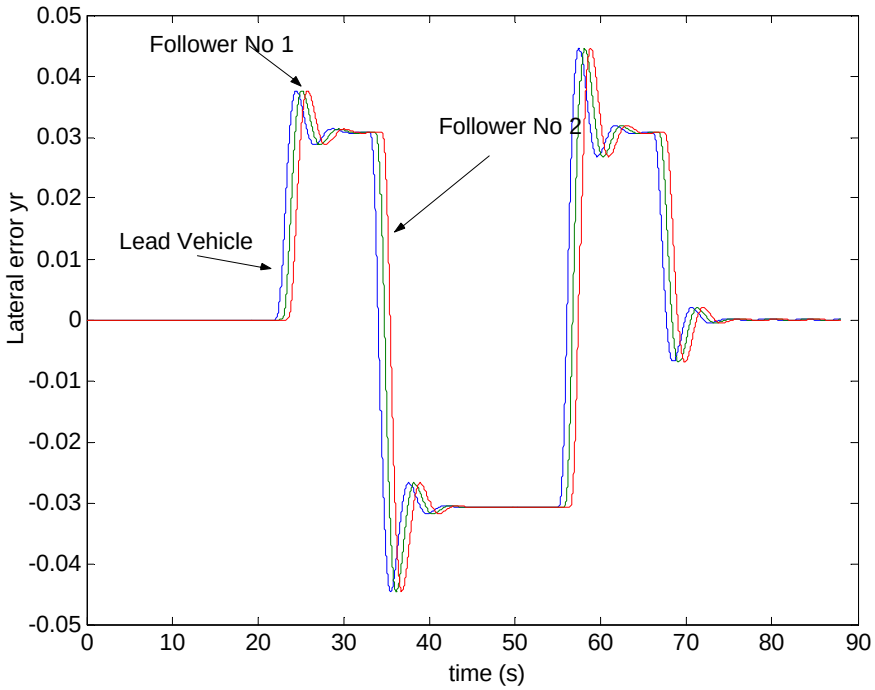

Fig. 3.16: Simulation of two-unit vehicle platoon w/ ideal inter-vehicle communication.

It can be seen that the lateral error does not propagate along the platoon. Rather, the lateral error profile is the same for all the vehicles – which was expected since the vehicles are identical – with the only difference being that it is shifted in time depending on the inter-vehicle spacing and each vehicle's velocity. In other words, this time shift occurs because each vehicle enters the curve at different times.

Modeling Communication Delay

In the previous subsection, it was assumed that the control algorithm for each vehicle was triggered upon the simultaneous receipt of all the messages. However, this is not the case in real life. One important consideration is the communication delay, which is inherent in wireless systems and makes the selection of the means of communication a non-trivial problem, since it is a significant performance degrading factor, [32]. This delay is due to three factors:

(i) Transmission delay, which is usually negligible. It refers to the time associated with sending bits over the network. This delay can be determined by the system's bit rate. It is the time it takes for a bit to go from its source to its destination and it does not take into account packet losses or data collisions.

(ii) Delay due to packet losses. These are intermittent, and methods to study the effects of these delays on the stability of system are being explored. If the communicated message is corrupted, it will be dropped and treated like a packet loss. The control algorithm will use the latest data received, which is not going to be updated unless valid data is received.

(iii) Communication architectural delay, that is, delay associated with the selection of the architecture of the communication system. These delays consist of the amount of time the transmitted data has to wait in a buffer before being used in by the control loop.

The choice of the communication system that supports the exchange of information among vehicles is a challenging task. Practically, there are two categories of communication systems, [16]: (i) Line-of-sight systems and (ii) Radio-based systems. As far as the former are concerned, they are based on the use of a pair of infrared or LASER transmitters/receivers that establish one-to-one communication between the vehicles. Their great disadvantage is that communication is lost once one of the devices is out of visual contact with the other. It is also interesting to note that if a message from the lead vehicle needs to be conveyed to a vehicle in the platoon, it has to hop from vehicle to vehicle to get to its destination.

In terms of radio-based communication systems, they require a networking protocol to prevent simultaneous transmissions from interfering with each other. Radio frequencies in the GHz range are chosen to support inter-vehicle communications due to the high data rate that is required. The most widely accepted protocol for inter-vehicle communication is the token-passing protocol. In this configuration, each vehicle broadcasts its ID with its data. The ID numbers are based on the position that the vehicle occupies in the platoon. To start the token passing protocol, the lead vehicle broadcasts its information on the channel, and starts a timer. Each following vehicle broadcasts its information only after receiving the broadcast of the vehicle immediately in front of it. When the last vehicle in the platoon has broadcast, the lead vehicle restarts the cycle. The amount of time that a user gets to transmit during the token cycle is called the time slot t_s and its size depends on the platoon size. Clearly, this configuration yields deterministic architecture delays, which make it very attractive for real time control applications.

An important control design decision that has to be made is the interface between the communication system and the controller. First of all, it should be noted that the token cycle time has to be at most equal to the sampling time of the monitoring device. Second,

the control strategy has to be decided. One possible idea is to trigger the control law once the information from the preceding vehicle is received. This means that the *i*th vehicle receives real time information from the preceding vehicle, and delayed information from vehicles *i-2, i*-3,…1, since these vehicles broadcast their data during the previous time slots. Specifically, data from the *i-2*th vehicle pertains to its position at time t-t_s, data from the *i-3*th vehicle pertains to its position at time t-$2t_s$ etc. This means that Eq. (3-21) becomes:

$$\begin{aligned} y_{s1}^{(i)} = \sum_{k=1}^{i} m_1^{(k)}\{t-kt_s\} - \left(x_p + d_s + d_1 + d_3\right)\sum_{k=1}^{i-1}(i-k)\,m_2{}^{(k)}\{t-kt_s\} - \\ -\sum_{k=1}^{i-1}\left[\left(x_p + d_s + d_1 + d_3\right)(i-k) - d_3\right] m_3{}^{(k)}\{t-kt_s\} \end{aligned} \tag{3-25}$$

Clearly, the interconnection among the vehicles is not eliminated and hence lateral platoon stability analysis will have to be conducted

On the other hand, if the control law is triggered upon receipt of the lead vehicle information, then all vehicles take their measurements simultaneously, thus creating a true "snapshot" of their positions at a certain moment, say t_k. Obviously, they cannot use these measurements in this control iteration because they cannot wait till all the vehicles take the token (till the cycle is completed). So they use the "snapshot" taken at time $t_{k-1.}$ (which was passed on to everybody in the time slot between t_k and t_{k-1}). This means that each vehicle is still "disconnected" from the rest of the vehicles, but there is just a delay in the measurements

$$\begin{aligned} y_{s1}^{(i)} = \sum_{k=1}^{i} m_1^{(k)}\{t-t_d\} - \left(x_p + d_s + d_1 + d_3\right)\sum_{k=1}^{i-1}(i-k)\,m_2{}^{(k)}\{t-t_d\} - \\ -\sum_{k=1}^{i-1}\left[\left(x_p + d_s + d_1 + d_3\right)(i-k) - d_3\right] m_3{}^{(k)}\{t-t_d\} \end{aligned} \tag{3-26}$$

where $t_{k-1} - t_k = t_d$. This delay can be taken care of by the controller. Indeed, the system is still "disconnected" and the communication delay introduces negligible performance deterioration.

This concludes the solution to the analytical part of the problem that was posed in the Introduction. The autonomous following system has been designed and it has been shown that lateral error propagation can be prevented by use of inter-vehicle communication, which eliminates the interconnection among the vehicles even when communication delay enters the system. As far as the implementation part is concerned, it is described in detail in Chapter 4.

4. IMPLEMENTATION

In this chapter, the implementation issues are discussed and some experimental results are presented. As discussed in Chapter 3, the components needed to implement lateral autonomous following are the following: (i) a device that monitors the rear end of the preceding vehicle, (ii) a communication system implementing a token-bus protocol, (iii) computing power to process the data and output the desired steering, (iv) a steering actuator to execute the controller command.

It has to be admitted that, due to several reasons, namely, the unavailability of the vehicles and the difficulty of integrating several subsystems, sensors, communication system etc., the experimental results are not thorough enough to completely validate the analytical ones.

4.1 Hardware

It was decided to use a passenger vehicle, namely a Buick LeSabre provided by California PATH, see Fig. 4.1, because the heavy duty trucks were being prepared for the Demo 2003.

Fig. 4.1: Experimental vehicle

To monitor the rear end of the preceding vehicle, a laser scanning radar (LIDAR) was installed on the front bumper of the vehicle, as shown in Fig. 4.2.

Fig. 4.2: The laser scanning radar (LIDAR)

The laser scanning radar (LIDAR), manufactured by Mitsubishi Electric Corp., Japan contains three components: the sensor head, the electronic control unit and the interfacing circuits. It sweeps an angle of *12°* (divided into *80* incremental segments) every *100ms*. The sensor emits laser pulses and employs a time-of-flight technique to calculate the polar distance to the object from which the signal reflected. The sensor can also read the intensity of the signal as it is reflected back from its surrounding environment. This has proved very useful in terms of facilitating the rejection of clutter and ghost targets. More details on the algorithm that was used are presented in the next subsection.

As far as the communication system is concerned, a “Utilicom/Hughes System” was used. It implements a token-bus protocol with token cycle of *20ms*. The system was successfully implemented in the NAHSC DEMO 1997 in San Diego for longitudinal control. The setup is very efficient for platoon sizes up to ten vehicles. Unfortunately the platoon size is pre-programmed, and the platoon size can not be changed dynamically. This is a disadvantage since in an AHS environment, cars will possibly be joining onto and/or splitting from platoons resulting in changes to the platoon size. However, for demonstration purposes it is sufficient.

Fig. 4.3: Antenna for inter-vehicle communication

In terms of computing power, two computers were used, one for data and program storage, located in the trunk of the vehicle and the other for implementing the real-time control (located next to the driver seat).

Fig. 4.4: On-board computers

It is noted that the trunk is loaded with several interface modules for the various other sensors that it is equipped with (longitudinal control radar, magnetometers, gyrometer, accelerometer etc).

Finally, the steering actuator is mounted on the steering column along with an encoder. This subsystem also includes the torsion bar, the hydraulic assist unit and a control algorithm that receives the desired steering angle from the steering controller and makes sure that the tires follow exactly this command. Recall that the controller was designed to control the steering angle of the wheels directly, and not of the steering

column; hence this “inner loop” is imperative for the implementation of the designed system, since it actually accounts for the steering subsystem dynamics.

It is noted that for two-unit vehicles the implementation of the control algorithm that was derived in Chapter 3, an additional encoder that measures the angle of rotation of the hitch is required. This is actually the yaw angle e_f of the trailer relative to the tractor’s reference frame, which is needed in order to compensate for trailer off-tracking.

4.2 Software

The software running on both computers is rather complicated since it needs to be generic enough to incorporate various control schemes, even those that require road infrastructure. Briefly speaking, a large number of processes run “simultaneously” and there is a database, where all the sensory data is stored in real time. Thus when an algorithm requires sensor information, it accesses the database through the use of triggers. The entire program is written in C Programming Language and the real-time operating system is QNX.

For the purposes of autonomous following, an important part of the software is the algorithm that processes the data from the LIDAR. As mentioned above, the LIDAR measures the time of flight of 80 pulses that are emitted and reflected back, and calculates the polar distance of the object corresponding to each pulse. In order to determine which pulses were reflected from the rear end of the preceding vehicle and which came from reflective clutter a Probabilistic Data Association Filter (PDAF) is used. The PDAF algorithm utilizes a probabilistic weighting window to validate possible candidate targets from the raw data. The algorithm eliminates the readings outside of the candidate window even if they are of high intensity. Next, it processes the remaining candidates to determine which reading(s) came from the intended target. Therefore, the algorithm can filter out reflective clutter and possible “ghost” targets (i.e. reflective objects which are *not* the intended tracking object). For further details on the PDAF algorithm, the reader is encouraged to refer to [38].

The PDAF algorithm has been shown in experiments to accurately track the relative movement of a reflective object. In autonomous following it is intended to monitor the preceding vehicle’s taillights. The estimated polar distance of each taillight is converted to Cartesian coordinates and hence the lateral distance of the preceding vehicle’s rear end center from the LIDAR can be interpolated. Additionally, by knowing

the location of these two points on the preceding vehicle the task of calculating the relative yaw angle between the controlled and the preceding vehicle is trivial. Recall that this variable is actually $\left(e_r^{(2)} - e_r^{(1)} - e_f^{(1)}\right)$ for two-unit vehicles, and $\left(e_r^{(2)} - e_r^{(1)}\right)$ for single-unit vehicles and the control algorithm needs it in both cases, see Section 3.4.

As far as the controller is concerned, it is clear that, since it is implemented in a digital computer, it needs to be transformed in the discrete time domain. Therefore, a Tustin transformation with a sampling time of *100ms* (equal to that of the LIDAR) is conducted for Eq. (3-7) and (3-8). The resulting discrete time controllers are shown below.

$$u(k) = 0.249y(k) - 0.463y(k-1) + 0.214y(k-2) + \\ +1.768u(k-1) - 0.771u(k-2) \tag{5-1}$$

$$u(k) = 0.574y(k) + 0.165y(k-1) - 0.972y(k-2) - 0.147y(k-3) + 0.417y(k-4) - \\ -1.203u(k-1) + 0.477u(k-2) + 1.016u(k-3) + 0.306u(k-4) \tag{5-2}$$

Finally, for safety reasons the desired steering angle, calculated by the controller, is bounded in the software level to *+/-10°* and the steering angle rate is limited to *+/-25°/s.*

4.3 Validation Method

As discussed before, up to now the experimental results are not enough to validate the analytical results presented in Chapter 3. More specifically, it has not been made possible to conduct experiments with inter-vehicle communication. However, the controller was tested with the use of magnetometers. The experimental vehicles were equipped with magnetometers in the front and rear bumper (Fig. 4.5a), and the centerline of the test track, where the experiments are conducted, is implanted with magnets spaced at 1m from each other.

(a) **(b)**

Fig. 4.5: Magnetometers mounted on the front (a) and rear (b) bumper

The test track used was California PATH Richmond Field Station Test Track where vehicle speeds are restricted to *25mph*. It is shown in the next figure; taking a close look at it, it is possible to see the magnets implanted in the road centerline.

Fig. 4.6: Richmond Field Station Test Track.

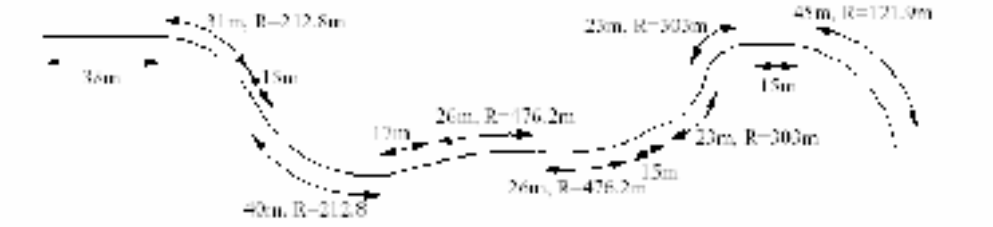

Fig. 4.7: Schematic of Richmond Field Station Test Track.

By use of front and rear magnetometers, it has been made possible to emulate the lidar/communication system to a certain extent. More specifically, as shown in Chapter 3, the lidar/communication system is basically a system that monitors the *exact* lateral error at a certain *look-ahead distance* with a certain *time delay*. The look-ahead distance was emulated by extrapolating the front and rear magnetometer measurements. As for the time delay, it was introduced in the control algorithm. To sum up, a look-ahead distance of *8m* was calculated and was fed into the controller and a time delay of *20ms* was hard-coded in order to account for the communication delay. Finally, although the magnetometers had a sampling frequency of 500Hz, the controller was updating the control action only every 100ms in order to emulate the 10Hz sampling frequency of the LIDAR. The results of the tests are shown in the next page.

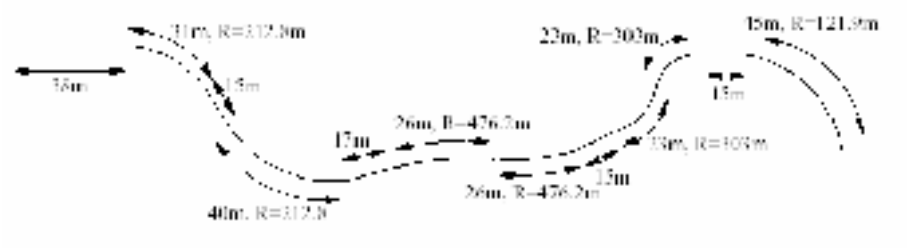

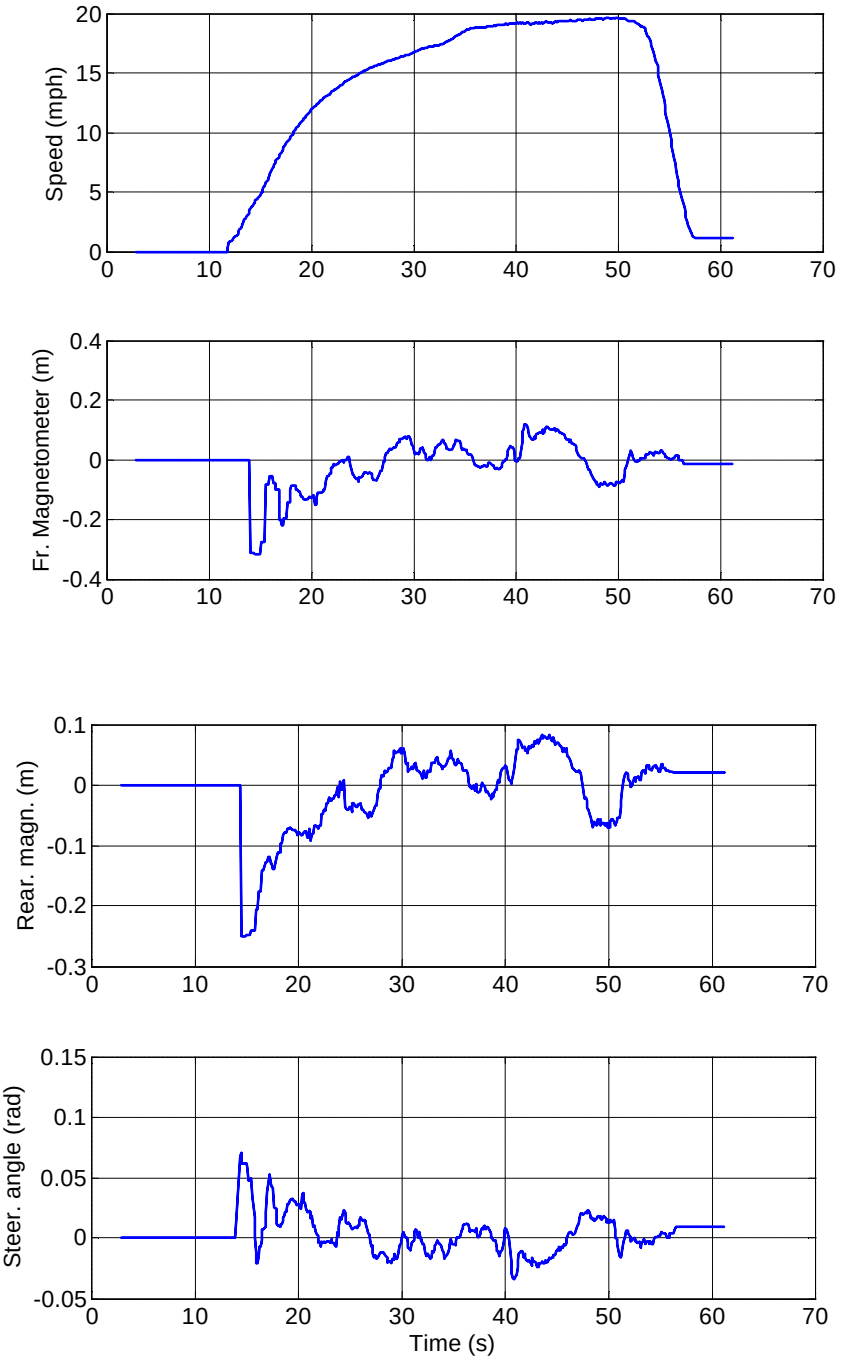

Fig. 4.8: Experimental Results.

It can be seen that the system performs acceptably, since it keeps the lateral error below 0.15m (apart from the first part, which was due to large initial error) in a test track with fairly high curvatures. It is important to say that this track does not have a straight part and thus the behavior of the system in terms of steady-state error could not be assessed.

5. CONCLUSIONS

This report concludes with the summary of the main results as well as suggestions for future work that will complement the research efforts towards fault tolerant automated highway systems.

5.1 Summary

This report focused on the development of automated highway systems without the use of road infrastructure. First, a unified approach to the dynamics of single-unit and two-unit vehicles was presented. A nonlinear dynamic model was derived under certain assumptions including negligible roll and pitch. For the purposes of control, the dynamic model was simplified to form a linear time invariant plant.

Next, the problem of autonomous following was considered. The influence of rear end off-tracking and look-ahead distance was illustrated and control methods were suggested, that address the limitations of autonomous following without inter-vehicle communication. Lateral platoon string stability was introduced and it was shown that interconnected platoons without inter-vehicle communication theoretically *can* be stable with the tradeoff of poor performance. Finally, it was shown that the addition of inter-vehicle communication ensures lateral platoon stability and satisfactory performance by eliminating the interconnection among the vehicles. This is feasible when the monitoring devices are triggered to take measurements simultaneously, so that they create "snapshots" of the vehicles' positions. Then, by communicating the sensor measurements, each vehicle is able to extract its position relative to lead vehicle thus eliminating any interconnection with the rest of the vehicles in the platoon. The communication delay is then viewed as a simple delay to a system that is completely independent of the platoon followers and hence does not affect platoon stability. Illustrative examples and simulations were used to verify the analytical results.

In terms of implementation, the entire hardware and software setup for autonomous following was shown. Few experiments were conducted mainly by emulating the performance of the LIDAR/communication system. Hence, the analytical results were

partially verified, but the success of the experiments motivates for the continuation of the experimental analysis.

In conclusion, it was shown that autonomous following lateral control of automated highway systems has several limitations; however it is a feasible alternative to infrastructure-dependent techniques and it can either assist them in faulty situations or under certain assumptions completely substitute for them.

5.2 Future Work

One of the most important stages that will lead to further development of the method is the experimental validation of autonomous following. More specifically, it is important that the communication system be set up so that it provides the variables needed to implement the controller that was designed. The measurements from the LIDAR and the communication system will unearth the limitations of this combination and the reliability of the scheme.

In terms of further extending the algorithms, autonomous following can benefit by the use of optimal and robust control techniques. Indeed, the designed controllers provide some robustness properties, but they are certainly not optimal. Establishing clear performance specifications and optimizing the controller is certainly an interesting area of research.

Finally, a challenging task is the integration of the autonomous following approach with techniques such as magnet-magnetometer based lateral control. This will increase the reliability of both systems. Sensor fusion is certainly within the scope of such a research effort.

REFERENCES

[1] Bernabeu, E.J., Tornero, J., Tomizuka, M., "Collision Prediction and Avoidance Amidst Moving Objects for Trajectory Planning Applications. Proc. of the 2001 IEEE Int. Conf. on Robotics and Automation, Korea, May 2001, pp.3801-3806.

[2] Bertozzi, M., Broggi, A., "Vision-based vehicle guidance", Computer, vol. 30, no.7, July 1997, pp.49-55.

[3] Betke, M., Haritaoglu, E., Davis, L. S., "Real-time multiple vehicle detection and tracking from a moving vehicle", Machine Vision & Applications, vol.12, no.2, 2000, pp.69-83. Springer-Verlag, Germany

[4] Bose., A., Ioannou, P., "Analysis of Traffic Flow with Mixed Manual and Semi-automated Vehicles", California PATH, Research Report UCB-ITS-PRR-99-14.

[5] Chee, W., Tomizuka, M., "Vehicle Lane Change Maneuver in Automated Highway Systems", California PATH Research Report, UCB-ITS-PRR-94-22, October 1994.

[6] Chen, C., "Backstepping Design of Nonlinear Control Systems and Its Applications to Vehicle Lateral Control in Automated Highway Systems", PhD Dissertation, Mechanical Engineering Department, University of California Berkeley, 1996.

[7] Chien, C., Ioannou, P., "Automatic Vehicle Following", Proc. of the Amer. Control Conf., Chicago, IL, July 1992, pp. 1748-1752.

[8] Choi, J. Y., et al "Vision Based Lateral Control By Yaw Rate Feedback", Proc. of the 27th Annual Conference of IEEE Industrial Electronics Society (IECON '01), pp. 2135 – 2138.

[9] Crisman, J. D., Rojas, J. C., "Vehicle detection in color images", IEEE Conference on Intelligent Transportation Systems. ITSC '97 Proceddings (Cat. No. 97TH8331). IEEE 1997, pp403-8. New York, NY, USA

[10] Daviet, P., Parent, M., "Longitudinal and Lateral Servoing of Vehicles in a Platoon", Proc. of the 1996 IEEE Intelligent Vehicles Symposium, 1996, pp. 41 – 46.

[11] Fraichard, T., "Dynamic Trajectory Planning with Dynamic Constraints: a 'State-Time Space' Approach", Proc. of the 1993 IEEE/RSJ Int. Conf. On Intellingent Robots and Systems, Yokohama, Japan, July 1993, pp. 1393- 1400.

[12] Gehring, O., Fritz, H., “Practical Results of a Longitudinal Control Concept for Truck Platoouning with Vehicle to Vehicle Communication”, IEEE Conference on Intelligent Transportation Systems, November 1997, Boston, MA, pp. 117-122.

[13] Gehring, S.K., Stein, F.J., “A Trajectory-Based Approach for the Lateral Control of Car Following Systems”, Proc. of the IEEE Int. Conf. on Systems, Man and Cybernetics, 1998, pp. 3596-3601.

[14] Gilbert, E.G., Johnson, D.W., Keerthi, S.S., “A Fast Procedure for Computing the Distance Between Complex Objects in Three- Dimensional Space”, IEEE Journal of Robotics and Automation, vol. 4, No. 2, April 1988, pp. 193-203.

[15] Godbole, D. N., Hagenmeyer, V., Sengupta, R., Swaroop, D., “Design of Emergency Maneuvers for Automated Highway System: Obstacle Avoidance Problem”, Proc. of the 36th Conf. on Decision and Control, San Diego, CA, December 1997, pp. 4474-4779.

[16] Hedrick, J.K., Chen, Y., Mahal, S., “Optimized Vehicle Control Communication Interaction in an Automated Highway System”, California PATH Research Report, UCB-ITS-PRR-2001-29.

[17] Hingwe, P., Wang, J.Y., Tai, M., Tomizuka, M., “Lateral Control of Heavy Duty Vehicles for Automated Highway Systems: Experimental Study on a Tractor Semi-Trailer”, California PATH working paper, UCB-ITS-PWP-2000-1, 2000

[18] Hingwe, P., et al. “Linear Parameter Varying Controller for Automated Lane Guidance-Experimental Study on Tractor Semi-Trailers”, Proc. of the American Control Conf., Chicago, IL, June 2000, pp. 2038 – 2042.

[19] Jacobs, P., and Canny, J., “Planning Smooth Paths for Mobile Robots”, Proc. of the IEEE Int. Conf. on Robotics and Automation, April 1989, pp. 2-7.

[20] Jula, H., Kosmatopoulos, E.B., Ioannou, P.A., “Collision Avoidance Analysis for Lane Changing and Merging”,IEEE Trans. on Vehicular Technology, vol. 49, No. 6, November 2000, pp. 2295-2308.

[21] Kanaris, A., Kosmatopoulos, E.B., Ioannou, P.A., “Strategies and Spacing Requirements for Lane Changing and Merging in Automated Highway Systems”, IEEE Transactions on Vehicular Technology, vol. 50, No. 6, November 2001, pp. 1568-1581.

[22] Kosecka, J., Blasi, R., Taylor, C.J., Malik, J., “Vision-Based Lateral Control of Vehicles”, The Confluence of Vision and Control, Springer-Verlag, 1998.

[23] Laugier, C., Paromtchik, I., Parent, M., “Developing Autonomous Maneuvering Capabilities for Future Cars”, Proc. 1999 IEEE/IEEJ/JSAI Int. Conf. on Intelligent Transportation Systems, Tokyo, Japan, October 1999, pp. 68-73.

[24] Laumond, J.P., Jacobs, J., Taix, M., Murray, R. M., “A Motion Planner for Nonholonomic Mobile Robots”, IEEE Tr. on Robotics and Automation, Vol. 10, No. 5, October 1994, pp. 577-593.

[25] Lee, G.D., Kim S.W., Yim, Y.U., Jung, J.H., Oh, S.Y., Kim, B.S., “Longitudinal and Lateral Control System Development for a Platoon of Vehicles”, Proc. of 1999 IEEE/IEEJ/JSAI Int. Conf. on Intelligent Transportation Syst., Tokyo, Japan, 1999, pp. 605-610.

[26] Liu, X., Mahal, S.S., Goldsmith, A., Hedrick, J.K., “Effects of Communication Delay on String Stability in Vehicle Platoons”, Proc. of 2001 IEEE Intelligent Transportation Systems Conf., Oakland, CA, August 2001, pp. 625-630.

[27] Lu, G., Tomizuka, M., “A Laser Scanning Radar Based Autonomous Lateral Vehicle Following Control Scheme for Automated Highways”, Proc. of the 2003 Amer. Control Conference, Denver, CO, June 2003.

[28] Papadopoulos, E., Poulakakis, I., Papadimitriou, I., “On Path Planning and Obstacle Avoidance for Nonholonomic Platforms with Manipulators: A Polynomial Approach”, International Journal of Robotics Research, Vol. 21, No. 4, 2002, pp. 367-383.

[29] Pomerleau, D., “Visibility estimation from a moving vehicle using the Ralph vision system”, IEEE Conference on Intelligent Transportation Systems. ITSC ’97 Proceedings (Cat. No. 97TH8331). IEEE 1997, pp906-11. New York, NY, USA

[30] Rajamani, R., et al. “A Complete Fault Diagnostic System for Automated Vehicles Operating in a Platoon”, IEEE Transactions on Control Systems Technology, vol 9, No. 4, July 2001, pp. 553-563.

[31] Scheuer, A., Fraichard, T., “Collision-Free and Continuous-Curvature Path Palnning for Car-Like Robots”, Proc. of the 1997 IEEE Int. Conf. On Robotics and Automation, Albuquerque, New Mexico, April 1997, pp. 867-873.

[32] Seiler, P., Sengupta, R., “Analysis of Communication Losses in Vehicle Control Problems”, Proc. of the American Control Conf., Arlington, VA, June 2001, pp. 1491-1496.

[33] Shiller, S., Sundar, S., “Optimal Emergency Maneuvers of Automated Vehicles” California PATH, Research Report UCB-ITS-PRR-96-32.

[34] Suryanarayanan, S., Howell, A., Yi, J., “Development and Implementation of a Vehicle-Centered Fault Diagnostic and Management System for the Extended PATH-AHS Architecture”, California PATH, TO 4207 Final Report.

[35] Suryanarayanan, S., “Fault Tolernat Control and its Application to Lane-Keeping Control of Auomated Vehicles”, PhD Dissertation, Mechanical Engineering Department, University of California Berkeley, 2002.

[36] Swaroop, D., Hedrick, J.K., “String Stability of Interconnected Systems”, IEEE Transactions on Automatic Control, vol 41, No 3, March 1996, pp. 349-357.

[37] Tai, M., “Advanced Vehicle Control of Heavy Vehicles for Automated Highway Systems”, PhD Dissertation, Mechanical Engineering Department, University of California Berkeley, 2001.

[38] White, R., Tomizuka, M., “Autonomous Following Lateral Control of Heavy Vehicles Using Laser Scanning Radar”, Proc. of the Amer. Control Conf., Arlington, VA, June 2001, pp. 2333-2338.

APPENDIX A

Vehicle Parameters used in simulations

Parameter	Value for tractor semi-trailer	Value for passenger vehicle
m_1	7700 *kg*	2100 *kg*
m_2	10500 *kg*	N/A
d_1	3.25 *m*	N/A
d_3	3.81 *m*	N/A
l_1	1.65 *m*	1.0 *m*
l_2	3.75 *m*	1.7 *m*
l_3	6.50 *m*	N/A
T_{w1}	2.02 *m*	N/A
T_{w2}	1.82 *m*	N/A
T_{w3}	1.82 *m*	N/A
I_{z1}	46000 $kg\text{-}m^2$	3214 $kg\text{-}m^2$
I_{z2}	162000 $kg\text{-}m^2$	N/A
C_{af}	180430 *N/rad*	60000 *N/rad*
C_{ar}	324774 *N/rad*	120000 *N/rad*
C_{at}	324774 *N/rad*	N/A
C_{lf}	127120 *N*	N/A
C_{lr}	4x108960 *N*	N/A
C_{lt}	4x95340 *N*	N/A
r_i	0.3 *m* (i=1,2,…,6)	N/A
I_{wi}	13.15 $kg\text{-}m^2$ (i = 1,2,…,6)	N/A

It is noted that the parameters marked N/A were either not available or not applicable to passenger vehicles.

APPENDIX B

MATLAB/Simulink Models

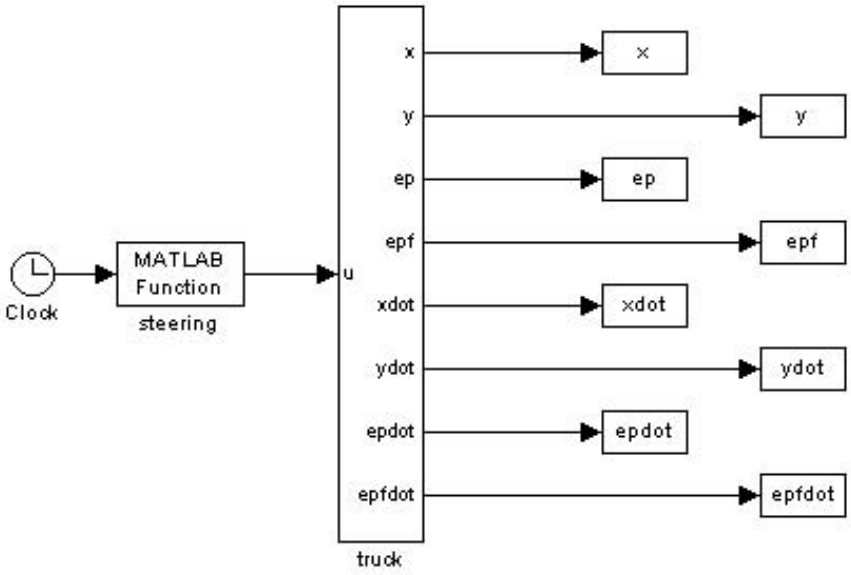

Fig. B.1: Heavy Vehicle Dynamic Model.

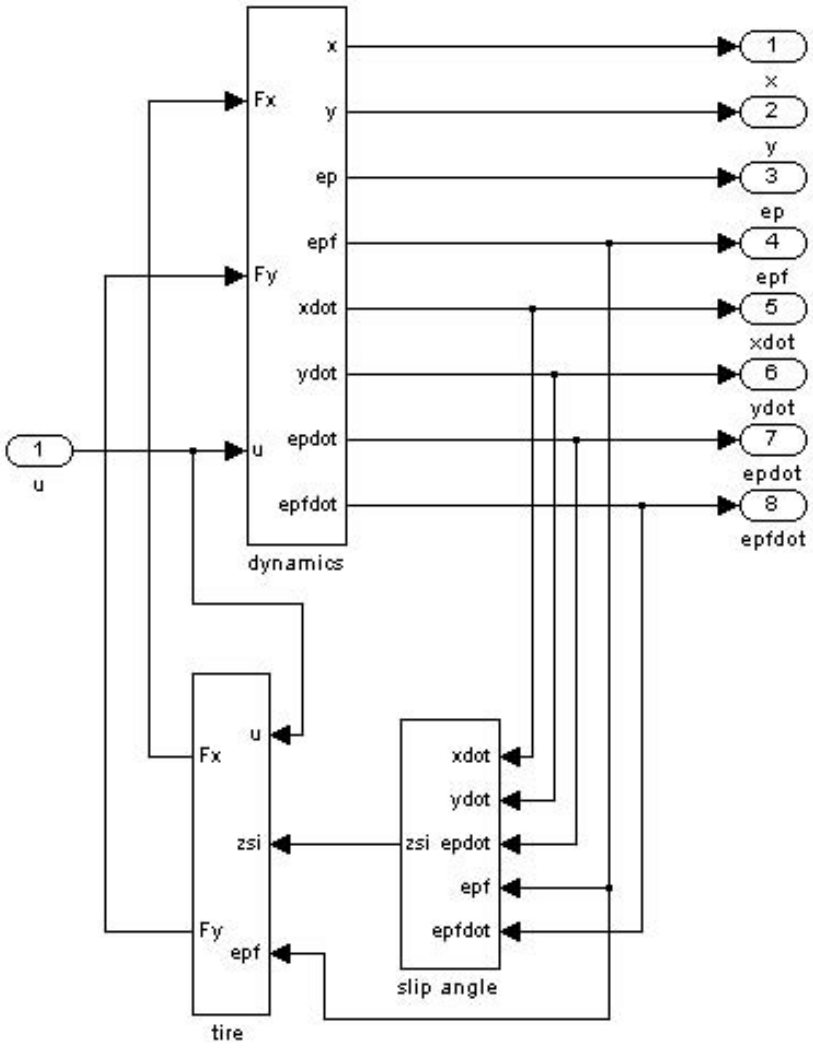

Fig. B.2: Heavy Vehicle Dynamic Model Subsystem.

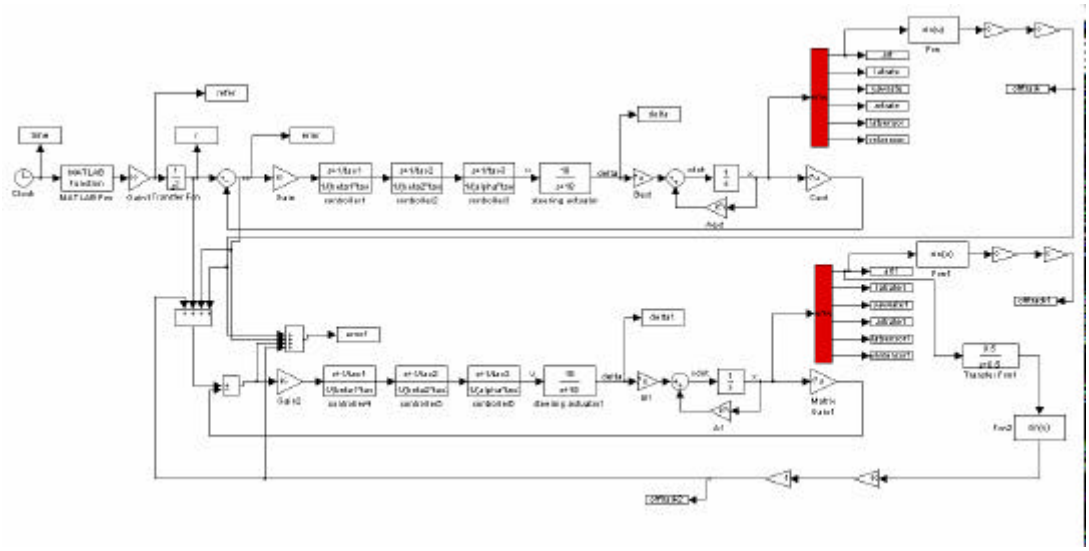

Fig. B.3: Platoon simulation 2 heavy vehicles.